

Electrically Small Planar Antenna for Circular Polarization

by

Johan Herman Huysamen

Thesis presented in partial fulfilment of the requirements for the degree of Master of Science in Engineering (Electronic Engineering with Computer Science) at the University of Stellenbosch



Department of Electric and Electronic Engineering
University of Stellenbosch
Private Bag X1, 7602 Matieland, South Africa

Supervisor: Prof K.D. Palmer

December 2006

Declaration

I, the undersigned, hereby declare that the work contained in this thesis is my own original work and that I have not previously in its entirety or in part submitted it at any university for a degree.

Signature:

J.H. Huysamen

Date:

Abstract

Electrically Small Planar Antenna for Circular Polarization

J.H. Huysamen

Department of Electric and Electronic Engineering

University of Stellenbosch

Private Bag X1, 7602 Matieland, South Africa

Thesis: MScEng (Electronic Eng with CS)

December 2006

The design of an electrically small planar antenna for compact circular polarization is presented. After an in-depth study of the performance limitations on electrically small antennas and an investigation into the working of various existing electrically small antennas, the design, simulation and measurement of the proposed antenna element is presented in detail.

Uittreksel

Elektries Klein Platvlak Antenna vir Sirkulêre Polarisasie

(“Electrically Small Planar Antenna for Circular Polarization”)

J.H. Huysamen

Departement Elektries en Elektroniese Ingenieurswese

Universiteit van Stellenbosch

Privaatsak X1, 7602 Matieland, Suid Afrika

Tesis: MScIng (Elektroniese Ing met RW)

Desember 2006

Die ontwerp van 'n elektries klein platvlak antenna vir kompakte sirkulêre polarisasie word voorgestel. Na 'n studie van die beperkte werkverrigting van elektries klein antennas en 'n ondersoek na die werking van verskeie bestaande elektries klein antennas, word die ontwerp, simulasie en meting van die voorgestelde antenna in detail bespreek.

Acknowledgements

I would like to express my sincere gratitude to the following people and organisations

Prof. Palmer for his insight and support and for our informative discussions,

Omnipless for their financial support,

Wessel Croukamp from SED for the construction of all antennas,

My parents for their support throughout my academic career and

Elsabé for all her love and support.

Dedications

Vir Elsabé. Vir altyd.

Contents

Declaration	i
Abstract	ii
Uittreksel	iii
Acknowledgements	iv
Dedications	v
Contents	vi
List of Figures	viii
List of Tables	xi
1 Introduction	1
2 Fundamental limitations in small antennas	3
2.1 Introduction	3
2.2 Relative size	4
2.3 Bandwidth and radiation Q	4
2.4 Gain	17
2.5 Efficiency	20
3 Electrically small antennas	26
3.1 Introduction	26
3.2 Multi-element monopole antenna	26

<i>CONTENTS</i>	vii
3.3 Loop fed spiral wire antenna	31
3.4 Dielectrically loaded patch antenna	35
3.5 Shorted probe fed microstrip antenna	37
3.6 Planar inverted-F antenna	38
4 Design of a sequentially rotated PIFA for circular polarization	41
4.1 Introduction	41
4.2 Specifications	41
4.3 Proposed design	41
4.4 Effect of the shorting pin as compared to a shorting plate	42
4.5 Effect of folding the antenna body	44
4.6 Sequential rotation for circular polarization	45
4.7 Design of the feed network	46
5 Simulated and measured results of the sequentially rotated PIFA	50
5.1 Introduction	50
5.2 Simulation	50
5.3 Construction	54
5.4 Measurement	56
5.5 Results	58
5.6 Q of the single folded PIFA	63
5.7 Arraying the antenna element	66
6 Conclusion	69
List of References	71

List of Figures

2.1	Schematic diagram of a vertically polarized omni-directional antenna.	5
2.2	Equivalent circuit of a vertically polarized omni-directional antenna.	6
2.3	Equivalent circuit of electric dipole. a is the radius of the sphere and c is the speed of light.	8
2.4	Equivalent circuit of TM_n spherical wave. a is the radius of the sphere and c is the speed of light.	8
2.5	Q for electrically small antennas as defined by Chu.	10
2.6	Q for electrically small antennas as defined by McLean.	14
2.7	Normal gain for electrically small antennas.	19
2.8	Percentage efficiency for aluminium and copper antennas versus relative size. The approximation becomes invalid for $kr > 1$.	22
2.9	Schematic of antenna with matching network.	23
3.1	Quarter-wave monopole antenna	27
3.2	Folded monopole antenna	27
3.3	Simulated s_{11} of the quarter-wave and folded monopole antennas	28
3.4	Simulated s_{11} for the folded monopole and top-loaded folded monopole antennas.	28
3.5	Goubau's broad-band multi-element monopole antenna.	29
3.6	Dimensions of the simulated Goubau antenna in m.	30
3.7	Simulated s_{11} of the Goubau antenna.	31
3.8	Design of the electrically small planar wire antenna.	32
3.9	Dimensions of antenna A in mm.	32
3.10	Simulated s_{11} for antenna A of figure 3.9	33
3.11	Lumped element circuit model.	33

3.12	Input impedance of the lumped element model and the simulated response.	34
3.13	Circular patch size against ϵ_r for $f_r = 1.6GHz$ and $h = 1.588mm$	36
3.14	Simulated s_{11} for circular patch antennas with various values of ϵ_r and $f_r = 1.6GHz$ and $h = 1.588mm$	36
3.15	Schematic of probe-fed patch with shorting post.	37
3.16	Simulated s_{11} of the probe-fed patch with shorting post.	38
3.17	E-field pattern for half-wave microstrip patch antenna.	39
3.18	Simulated s_{11} for the $\frac{\lambda}{2}$ patch and the $\frac{\lambda}{4}$ PIFA	40
4.1	Final design.	42
4.2	Simulated s_{11} of the pin-shortened and plate-shortened PIFA showing the reduction in resonant frequency.	43
4.3	Unfolded and folded versions of the PIFA	44
	(a) Unfolded	44
	(b) Folded	44
4.4	Simulated s_{11} for the unfolded and folded PIFA's.	45
4.5	Sequential rotation of the four elements.	46
4.6	Rotating field vector.	46
4.7	Layout of the feed network.	47
4.8	Simulated relative gain from input to each of the four arms of the feed network.	48
4.9	Simulated relative phase from input to each of the four arms of the feed network.	49
5.1	FEKO model of the antenna. Dimensions in m.	51
5.2	Simulated Right-hand (RHP) and Left-hand (LHP) polarized gain versus radiation angle.. . . .	52
5.3	Simulated s_{11} for single PIFA element.	52
5.4	Simulated s_{11} of the antenna connected to the feed network.	53
5.5	Final constructed antenna.	54
5.6	Antenna with conductive ground plane.	55
5.7	Measured s_{11} of the antenna input versus frequency.	57
5.8	Measured Right-hand (RHP) and Left-hand (LHP) polarized gain versus radiation angle.	57

LIST OF FIGURES

x

5.9	Measured and simulated right-hand and left-hand circularly polarized gain against theta at the center frequency of $1.541GHz$	59
5.10	Measured and simulated right-hand and left-hand polarized gain against theta at the upper limit of the frequency band at $1.562GHz$	60
5.11	Measured and simulated s_{11} for the antenna.	61
5.12	Simulated s_{11} for the antenna with an infinite and a finite ground plane.	62
5.13	Equivalent circuit for the single folded PIFA.	63
5.14	Simulated impedance and impedance of the equivalent circuit for the single folded PIFA.	64
5.15	Q versus relative size for the folded PIFA and other electrically small antennas against the limits proposed by Chu and Mclean.	65
5.16	Simulation model of 9-element rectangular array.	66
5.17	Right-hand polarized gain for the single element and the 9-element rectangular array phase steered to $\theta = 45^\circ$	67
5.18	Right-hand polarized gain for the single element and the 9-element rectangular array phase steered to $\theta = 85^\circ$	68

List of Tables

4.1	Antenna design specifications	42
-----	---	----

Chapter 1

Introduction

The objective is to design an electrically small circularly polarized patch-type element to be used in a phase-steered array antenna.

Patch antennas are considered as physically constrained because of their limited height. It is this limitation in height that makes these antennas ideal for use on aircraft as their low profile reduces the aerodynamic drag they produce. In the defence industry this low profile has the added advantage of reducing the radar signature of the aircraft.

This reduction in height makes the patch antenna an inherently narrow-band structure. Further reduction in the overall size of the patch will have a significantly detrimental effect on the bandwidth and this, along with the reduced efficiency, is one of the main concerns in the design of electrically small patch antennas.

An intensive study of the theoretical effects of antenna size on the performance of electrically small antennas is presented. The effect of antenna size on gain, bandwidth and efficiency is considered and the concept of fundamental limits on these three performance indices is presented.

Next various electrically small planar and patch-type geometries are considered. The performance of these antennas are critically examined.

A four element array of sequentially rotated folded Planar Inverted-F Antennas (PIFA's) is proposed to meet the design goals. The PIFA is chosen as this geometry halves the size of a resonant patch by the simple addition of a shortening post. Circular polarization is achieved by using four rotated and sequentially fed PIFA's. To ensure that the whole structure is electrically small each of these PIFA's has to be folded to halve their size once more. This results in an antenna consisting of four sequentially rotated, folded PIFA's, each approximately an eighth of the free-space wavelength in size. Thus the whole antenna is a quarter-wave structure, which qualifies it as electrically small.

The design and construction of this antenna is related along with simulated and measured results to confirm that the proposed design meets the design goals.

Chapter 2

Fundamental limitations in small antennas

2.1 Introduction

In all areas of engineering it is the responsibility of the engineer to strike a balance between performance and the cost associated with that performance. In general performance is directly proportional to cost and the relation is quite intuitive. But in some cases a small increase in performance comes at a largely increased cost. It was stated by Hansen (1) that when a much higher performance is needed the cost may increase exponentially. In such a case the performance is said to have a fundamental limit.

The purpose of an antenna is to couple to a free space wave. As such there is a limit on the size reduction of antennas. The performance indices of bandwidth, gain and efficiency are closely related to the cost factor of size.

Size reduction has long been the norm in many areas of electronic engineering. In the area of consumer electronics size reduction has become a very successful marketing strategy and the consumer has come to expect new electronic devices to be smaller than their predecessors. As such the antennas on cellular phones, GPS's and satellite phones have become smaller and smaller, but at what cost in terms of performance?

In the aeronautical and space industries small antennas are valued highly for their cost-effective use of space and their reduced aerodynamic interference. But a

small antenna with insufficient bandwidth and gain would necessitate extra matching and gain stages which would, in themselves, require more space.

With this in mind the antenna designer must strike a balance between size and performance. In the past much has been written on the effect of an antenna's size on its performance by the likes of Wheeler (2), Chu (3), Harrington (4) and others (5; 6) and more recently by McLean (7), Grimes and Grimes (8) and Thiele (9). In this chapter quantitative relationships between the cost factor of size and the three performance indices of bandwidth, gain and efficiency are investigated.

2.2 Relative size

The concept of relative size is used to relate the physical size of an antenna to the size relative to its operating frequency. The relative size is defined as kr , where the free-space wave number k is given by

$$k = \frac{2\pi}{\lambda} \quad (2.2.1)$$

and r is the radius of the smallest sphere that includes the whole antenna.

To be defined as electrically small an antenna must have a relative size of $kr \leq 1$. This relates into a radius of $r \leq \frac{\lambda}{2\pi}$

2.3 Bandwidth and radiation Q

RF devices are mostly used to transmit data in a standardized format and in these cases the transmission bandwidth is predetermined. Reducing the size of an antenna reduces the bandwidth and, for the given bandwidth, there is a fundamental lower limit on the size of the antenna. Much work has been done on the relation between antenna size and Q-factor. The Q-factor is the relation between the stored energy and radiated power of the antenna. In general the Q-factor is taken to be the reciprocal of the half-power bandwidth. This relation is not accurate for electrically small antennas, but a lower Q-factor is still taken to mean a wider bandwidth.

For that reason two popular derivations of the fundamental limit on radiation Q-factor, and indirectly bandwidth, are given here. The first is the equivalent circuit derivation proposed by Chu (3) and the second is the direct derivation proposed by McLean (7). Next a more accurate relation of Q-factor to bandwidth proposed by Fante (6) is examined.

2.3.1 Derivation of radiation Q from equivalent circuit of the spherical waves

As stated by Harrington (4) radiation Q is generally defined as

$$Q = \begin{cases} \frac{2\omega W_e}{P_{rad}} & W_e > W_m \\ \frac{2\omega W_m}{P_{rad}} & W_m > W_e \end{cases}, \quad (2.3.1)$$

with W_e the time-average, non propagating, stored electric energy, W_m the time-average, non propagating, stored magnetic energy, ω the frequency in radians and with P_{rad} the radiated power.

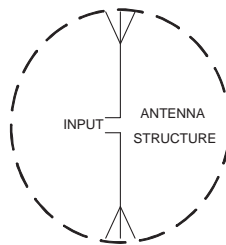


Figure 2.1: Schematic diagram of a vertically polarized omni-directional antenna.

Chu (3) considered a vertically polarized, omni-directional antenna lying within a spherical surface of radius $r = a$ as shown in figure 2.1. The field outside the sphere is expressed in terms of a complete set of orthogonal, spherical waves, propagating radially outward. The circularly symmetrical field can be described using only TM_{n0} waves.

As the energy is not linear in the field components, Chu had difficulty separating the energy associated with the local field from the radiated energy. To overcome this, the field problem was reduced to a circuit problem with the radiation loss replaced by a conduction loss.

As a result of the orthogonal properties of the spherical wave functions, the total energy stored outside the sphere is equal to the sum of the energies associated with each spherical wave and the complex power transmitted across the surface of the sphere is equal to the sum of the complex powers of each spherical wave. There is no coupling between the spherical waves outside the sphere. This enabled Chu to replace the space outside the sphere with a number of independent equivalent circuits. The number of equivalent circuits is equal to the number of spherical waves needed to describe the field outside the sphere.

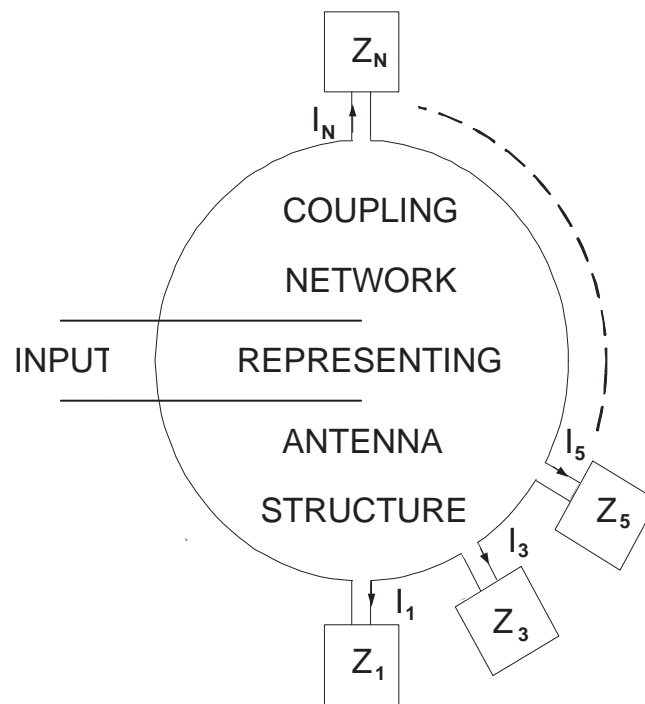


Figure 2.2: Equivalent circuit of a vertically polarized omni-directional antenna.

three elements shown in figure 2.3. This circuit represents a wave which could be generated by a infinitesimally small dipole.

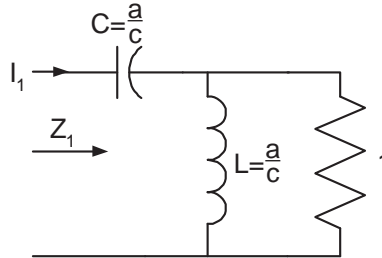


Figure 2.3: Equivalent circuit of electric dipole. a is the radius of the sphere and c is the speed of light.

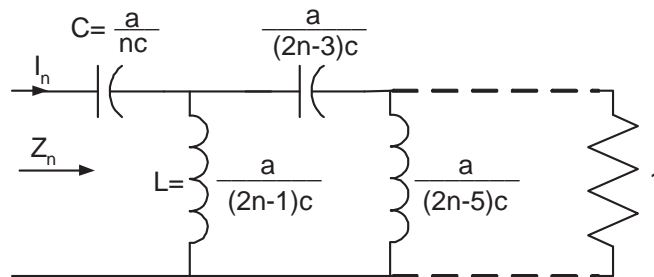


Figure 2.4: Equivalent circuit of TM_n spherical wave. a is the radius of the sphere and c is the speed of light.

The equivalent circuit for Z_n is shown in figure 2.4. The dissipation in the resistance is equal to the radiation loss of the antenna. The capacitances and inductances are proportional to the ratio of the radius of the sphere to the speed of light. As it would be tedious to calculate the total electric energy stored in all the capacitances of the equivalent circuit, Chu approximated the circuit by a simple series RLC circuit with similar frequency behavior close to the operating frequency. R_n , C_n and L_n of the simplified equivalent circuit are calculated by equating the resistance, reactance and the frequency derivative of the reactance to those of the series RLC circuit. The following results are obtained:

$$\begin{aligned}
R_n &= |kah_n(ka)|^{-2} \\
C_n &= \frac{2}{\omega^2} \left[\frac{dX_n}{d\omega} - \frac{X_n}{\omega} \right]^{-1}, \\
L_n &= \frac{1}{2} \left[\frac{dX_n}{d\omega} + \frac{X_n}{\omega} \right]
\end{aligned} \tag{2.3.4}$$

where $X_n = [kaj_n(kaj_n)' + kan_n(kan_n)'] |kah_n(ka)|^{-2}$, and j_n and n_n are the spherical Bessel functions of the first and second kind. From the simplified equivalent circuit the average power dissipation in Z_n is

$$P_n = \left(\frac{\mu}{\epsilon} \right)^{\frac{1}{2}} \frac{2\pi n(n+1)}{2n+1} \left(\frac{A_n}{k} \right)^2. \tag{2.3.5}$$

The average electric energy stored in Z_n is given in equation (2.3.6). It is larger than the average stored magnetic energy.

$$W_n = \left(\frac{\mu}{\epsilon} \right)^{\frac{1}{2}} \frac{\pi n(n+1)}{2(2n+1)} \left(\frac{A_n}{k} \right)^2 |kah_n(ka)|^2 \left[\frac{dX_n}{d\omega} - \frac{X_n}{\omega} \right]. \tag{2.3.6}$$

Next Q_n for the TM_n wave is calculated as

$$Q_n = \frac{2\omega W_n}{P_n} = \frac{1}{2} |kah_n(ka)|^2 \left[ka \frac{dX_n}{d(ka)} - X_n \right]. \tag{2.3.7}$$

Hansen (1) stated that when multiple modes are supported, the overall Q is

$$Q = \frac{\sum_{n=1}^N \frac{a_n a_n^* Q_n}{(2n+1)}}{\sum_{n=1}^N \frac{a_n a_n^*}{(2n+1)}}. \tag{2.3.8}$$

with a_n the excitation coefficient of the n th mode. As the higher order modes become evanescent with $ka < 1$, it can be shown that the Q becomes:

$$Q = \frac{1 + 3k^2 a^2}{k^3 a^3 (1 + k^2 a^2)}. \quad (2.3.9)$$

In figure 2.5, Q is plotted against ka over the range that constitutes an electrically small antenna. It is clear that as the relative size of the antenna is decreased there is an exponential increase in the Q-factor. This translates into a sharp decrease in the achievable bandwidth.

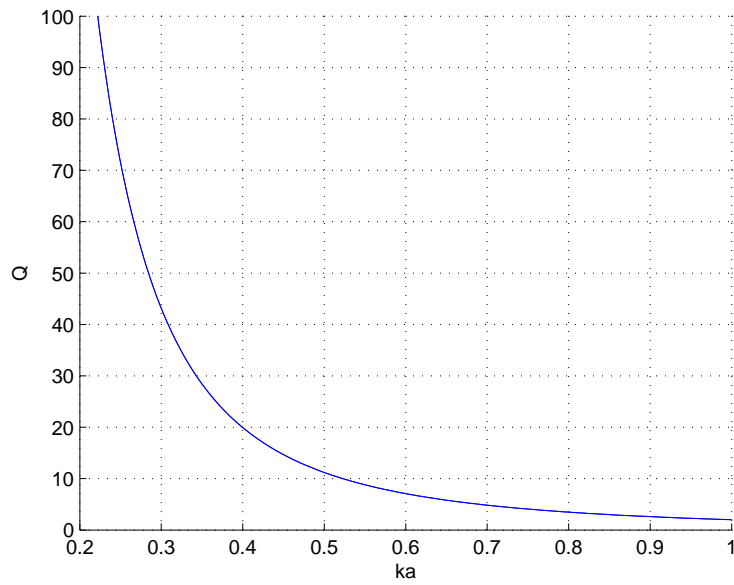


Figure 2.5: Q for electrically small antennas as defined by Chu.

2.3.2 Exact derivation of radiation Q from non propagating energy

McLean (7) proposed an exact method for calculating the radiation Q of a general antenna from the non propagating energy. McLean obtains the fields of the TM_{01} spherical mode from the r-directed magnetic vector potential, A_r as taken from Harrington (10).

$$A_r = -\cos\theta e^{-jkr} \left(1 - \frac{j}{kr}\right) \quad (2.3.10)$$

$$H_\phi = \sin\theta e^{-jkr} \left(\frac{j}{kr^2} - \frac{1}{r}\right) \quad (2.3.11)$$

$$E_\theta = \frac{1}{j\omega\epsilon} \sin\theta e^{-jkr} \left(-\frac{1}{r^2} - \frac{jk}{r} + \frac{j}{kr^3}\right) \quad (2.3.12)$$

$$E_r = \frac{1}{\omega\epsilon} 2\cos\theta e^{-jkr} \left(\frac{1}{kr^3} + \frac{j}{r^2}\right) \quad (2.3.13)$$

The field components are taken as RMS and from them the electric- and magnetic-energy densities, ω_e and ω_m , are calculated.

$$\begin{aligned} \omega_e &= \frac{1}{2}\epsilon \vec{E} \bullet \vec{E}^* \\ &= \frac{1}{2}\epsilon (|E_\theta|^2 + |E_r|^2) \\ &= \frac{1}{\omega} \eta \frac{1}{2} \left[\sin^2\theta \left(\frac{1}{k^3 r^6} - \frac{1}{kr^4} + \frac{k}{r^2}\right) + 4\cos^2\theta \left(\frac{1}{k^3 r^6} + \frac{1}{kr^4}\right) \right] \end{aligned} \quad (2.3.14)$$

$$\begin{aligned}
\omega_m &= \frac{1}{2}\mu\vec{H} \bullet \vec{H}^* \\
&= \frac{1}{2}\mu |H_\phi|^2 \\
&= \frac{1}{2}\mu \sin^2 \theta \left(\frac{1}{k^2 r^4} + \frac{1}{r^2} \right)
\end{aligned} \tag{2.3.15}$$

with $\eta = \sqrt{\mu/\epsilon}$.

The electric-energy density associated with the traveling wave, ω_e^{rad} , is calculated from the radiating field components.

$$H_\phi^{rad} = -\sin \theta \frac{e^{-jkr}}{r} \tag{2.3.16}$$

$$E_\theta^{rad} = -\eta \sin \theta \frac{e^{-jkr}}{r} \tag{2.3.17}$$

$$\omega_e^{rad} = \frac{1}{2}\epsilon |E_\theta^{rad}|^2 = \frac{\eta^2}{r^2} \sin^2 \theta \tag{2.3.18}$$

The non propagating electric-energy density, ω_e' , is the difference between the total and the propagating electric-energy densities.

$$\omega_e' = \omega_e - \omega_e^{rad} = \frac{\eta}{2\omega} \left[\sin^2 \theta \left(\frac{1}{k^3 r^6} - \frac{1}{kr^4} \right) + 4 \cos^2 \theta \left(\frac{1}{k^3 r^6} + \frac{1}{kr^4} \right) \right] \tag{2.3.19}$$

The total non propagating electric energy, W_e' , is obtained by integrating 2.3.19 over the volume outside the sphere with radius a containing the antenna.

$$\begin{aligned}
W'_e &= \int_0^{2\pi} \int_0^\pi \int_a^\infty \omega'_e r^2 \sin \theta dr d\theta d\phi \\
&= \frac{4\pi\eta}{3\omega} \left[\frac{1}{k^3 a^3} + \frac{1}{ka} \right]
\end{aligned} \tag{2.3.20}$$

The total radiated power is obtained by integrating the real part of the Poynting vector over a spherical surface.

$$\begin{aligned}
P_{rad} &= \int_0^{2\pi} \int_0^\pi \operatorname{Re} (\mathbf{E} \times \mathbf{H}^*) \cdot \hat{a}_r r^2 \sin \theta d\theta d\phi \\
&= \frac{8\pi}{3} \eta
\end{aligned} \tag{2.3.21}$$

From these the quality factor is obtained. As can be seen from figure 2.6 the relation between Q-factor and relative size is similar to that of the previous section.

$$Q = \frac{2\omega W'_e}{P_{rad}} = \frac{1}{k^3 a^3} + \frac{1}{ka} \tag{2.3.22}$$

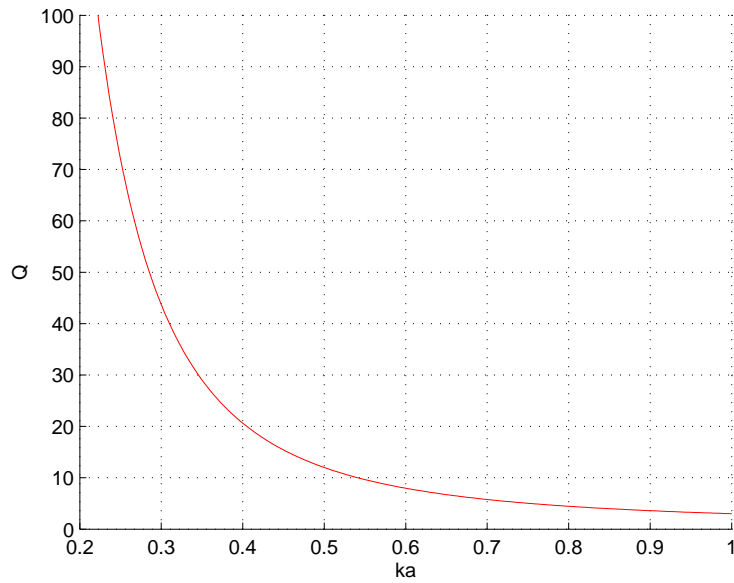


Figure 2.6: Q for electrically small antennas as defined by McLean.

2.3.3 Relation between Bandwidth and Q-factor

In general the radiation Q-factor of an antenna is taken to be the reciprocal of its half-power bandwidth. This assumption is not accurate for electrically small antennas.

Fante (6) defined the relation between Q-factor and fractional bandwidth. The input impedance of an antenna system, as taken from Harrington (10), was considered.

$$Z = R + jX = \frac{1}{|I|^2} [P_{rad} + j2\omega (W_m - W_e)] \quad (2.3.23)$$

Based on circuit theory Fante assumed that, for a high-Q system with resonance at ω_0 , $(\frac{dR}{d\omega})_{\omega_0} \approx 0$ and $X(\omega_0) = 0$. Just off resonance Z can be written as

$$Z \approx R + j(\omega - \omega_0) \left[\frac{dX}{d\omega} \right]_{\omega_0} + \dots \quad (2.3.24)$$

At the half-power points $\left|(\omega - \omega_0) \left(\frac{dX}{d\omega}\right)_{\omega_0}\right| = R$ and the fractional bandwidth B can then be written as

$$B \approx \frac{2R}{\omega_0 \left(\frac{dX}{d\omega}\right)_{\omega_0}} = \frac{2P_{rad}}{\omega_0 |I|^2 \left(\frac{dX}{d\omega}\right)_{\omega_0}} \quad (2.3.25)$$

By extending the treatment of the frequency derivatives of Maxwell's equations by Harrington (4, pp 394-396) Fante evaluates $\left(\frac{dX}{d\omega}\right)$ as

$$\frac{\delta X}{\delta \omega} = \frac{2W}{|I|^2} - \frac{2}{\eta |I|^2} \text{Im} \int_{S_\infty} \left(\vec{E}_\infty \bullet \frac{\delta \vec{E}_\infty^*}{\delta \omega} \right) d\Omega \quad (2.3.26)$$

Using 2.3.26 in 2.3.25 we obtain

$$B \approx \left[\frac{\omega_0 W}{P_{rad}} + F(\omega_0) \right]^{-1} \quad (2.3.27)$$

where

$$F(\omega_0) = -\frac{\omega_0}{\eta P_{rad}} \text{Im} \int_{S_\infty} \left(\vec{E}_\infty \bullet \frac{\delta \vec{E}_\infty^*}{\delta \omega} \right) d\Omega$$

The total non propagating, stored energy, W , can be defined as the sum of the energy stored within the sphere of radius a that surrounds the antenna, W_{in} , and the non propagating energy outside this sphere, W_{out} . The Q-factor is then defined as $Q = \frac{\omega_0 W_{out}}{P_{rad}}$. 2.3.27 then becomes

$$B \approx \left[Q + \frac{\omega_0 W_{in}}{P_{rad}} + F(\omega_0) \right]^{-1} \quad (2.3.28)$$

Fante goes on to show that for high-Q antennas the $F(\omega_0)$ term is negligible. Inversely for low-Q antennas the $F(\omega_0)$ term along with the $\frac{\omega_0 W_{in}}{P_{rad}}$ term relating the stored energy within the sphere has an effect on the achievable bandwidth. This shows that, while the relation $B = \frac{1}{Q}$ does not always hold, a lower Q always implies a larger bandwidth. From this and the previous sections it is clear that there is a

lower limit on the achievable Q and thus an upper limit on the bandwidth of an antenna of a given size.

2.4 Gain

From Harrington (4) the directive gain at a distance r from the antenna is the ratio of the maximum density of outward directed power flux to the average power density.

$$G(r) = \frac{4\pi r^2 \text{Re}(S_r)_{max}}{\text{Re}(P)} \quad (2.4.1)$$

Here S_r is the radial component of the complex Poynting vector at distance r and P is the total outward-directed complex power. By expanding the field external to a sphere containing all sources in terms of spherical wave functions, Harrington derives the gain as

$$G = \frac{\text{Re}[(\sum_n a_n F_n + j b_n F'_n)(\sum_n b_n F_n + j a_n F'_n)^*]}{4 \sum_{m,n} \frac{n(n+1)(n+m)!}{\epsilon_m (2n+1)(n-m)!} (|A_{mn}|^2 + |\eta B_{mn}|^2)} \quad (2.4.2)$$

where $F_n(kr) = kr h_n^{(2)}(kr)$, $a_n = n(n+1)A_{1n}$, $b_n = \eta n(n+1)B_{1n}$ and A_{mn} and B_{mn} are the coefficients of the solutions to the Helmholtz equation. There is no limit to the gain if all orders of spherical wave functions are excited. A limit is created by restricting the orders to $n \leq N$. As only A_{1n} and B_{1n} contribute to the numerator of 2.4.2, the gain is increased by setting

$$A_{mn} = B_{mn} = 0 \quad m \neq 1. \quad (2.4.3)$$

As 2.4.2 is symmetrical in a_n and b_n , the maximum gain is achieved when

$$a_n = b_n. \quad (2.4.4)$$

This reduces 2.4.2 to

$$G = \frac{\operatorname{Re} \left[\left(\sum_{n=1}^N a_n u_n \right) \left(\sum_{n=1}^N a_n u_n \right)^* \right]}{4 \sum_{n=1}^N |a_n|^2 \frac{1}{2n+1}} \quad (2.4.5)$$

with

$$u_n(kr) = F_n(kr) + j\overline{F'_n(kr)}. \quad (2.4.6)$$

Next 2.4.5 is increased by setting $\angle a_n = -\angle u_n$ which leads to

$$G = \frac{\left(\sum_{n=1}^N |a_n| |u_n| \right)^2}{4 \sum_{n=1}^N |a_n|^2 \frac{1}{2n+1}}. \quad (2.4.7)$$

By requiring $\frac{\partial G}{\partial |a_i|} = 0$ for all $|a_i|$ the $|a_n|$ are adjusted for maximum gain. This yields

$$G(kr)_{max} = \frac{1}{4} \sum_{n=1}^N (2n+1) |u_n(kr)|^2. \quad (2.4.8)$$

This is the maximum gain achievable with wave functions of order $n \leq N$. In the far zone, where $kr \rightarrow \infty$, $|u_n|^2 \rightarrow 4$ and 2.4.8 reduces to

$$G(\infty)_{max} = \sum_{n=1}^N (2n+1) = N^2 + 2N. \quad (2.4.9)$$

The *normal gain* of an antenna is defined as the maximum gain obtainable by using only wave functions of order $n \leq N = kr$. Thus the normal gain of an antenna with radius R is given by

$$G_{norm} = (kR)^2 + 2kR \quad (2.4.10)$$

This normal gain is shown in figure 2.7 over the range that constitutes an electrically small antenna.

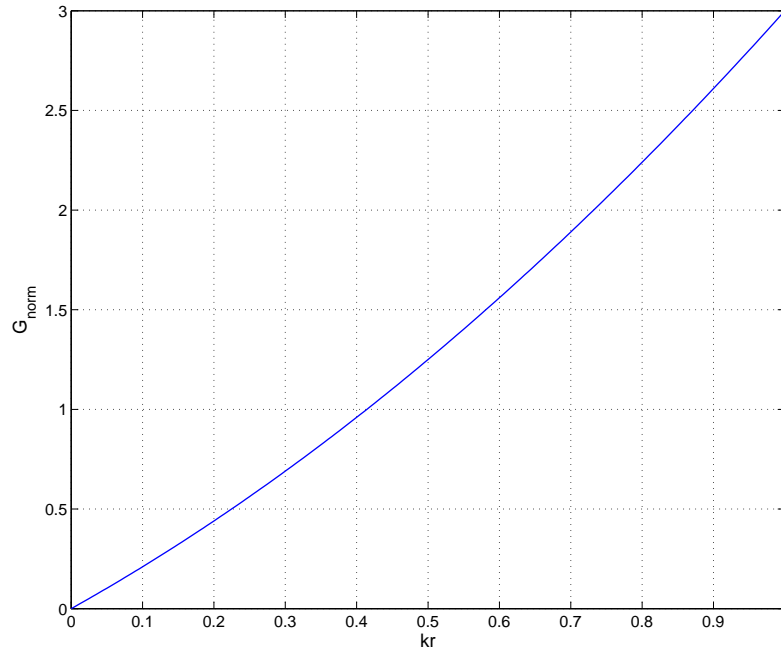


Figure 2.7: Normal gain for electrically small antennas.

A *supergain antenna* is one that achieves more gain than the normal gain by using more wave functions. As can be seen from 2.3.8 adding modes significantly increases the Q of an antenna and for that reason supergain antennas are very frequency sensitive. Thus, while there is no theoretical limit on the gain achievable, there is a limit on the gain of an antenna with a practical bandwidth.

2.5 Efficiency

The radiation efficiency of an antenna is defined as the ratio of the radiated power to the average power supplied to the antenna.

To define the fundamental limit on the radiation efficiency of an antenna Harrington (4) considers a spherical conductor of radius R excited by magnetic sources on its surface. The characteristic impedances for the various modes inside the sphere, $r < R$, are

$$Z_{mn}^{TE} = \frac{\eta_c}{\eta} \left[\frac{F_n(kr)}{jF'_n(kr)} \right]^* \approx \frac{\eta_c}{\eta} \quad (2.5.1)$$

$$Z_{mn}^{TM} = \frac{\eta_c}{\eta} \left[\frac{jF'_n(kr)}{F_n(kr)} \right]^* \approx \frac{\eta_c}{\eta} \quad (2.5.2)$$

with k the wave number and η_c the intrinsic impedance in the conductor,

$$k \approx (1 - j) \sqrt{\frac{\omega\mu\sigma}{2}} \quad \eta_c \approx (1 + j) \sqrt{\frac{\omega\mu}{2\sigma}} \quad (2.5.3)$$

Harrington defines the ratio of dissipated to radiated power as

$$\frac{P_{diss}}{P_{rad}} = \frac{|I_{mn}|^2 \operatorname{Re}(Z_{mn}^-)}{|I_{mn}|^2 \operatorname{Re}(Z_{mn}^+)} = \frac{\operatorname{Re}(\eta_c)}{\eta \operatorname{Re}(Z_{mn}^+)} \quad (2.5.4)$$

where Z_{mn}^- refers to the characteristic impedance within the spherical conductor and Z_{mn}^+ to the characteristic impedance outside the sphere. For equal TE_{mn} and TM_{mn} excitation Harrington defines the dissipation factors as

$$\begin{aligned} D_n &= \frac{P_{diss}^{TE} + P_{diss}^{TM}}{P_{rad}^{TE} + P_{rad}^{TM}} = \frac{P_{diss}^{TE}}{2P_{rad}^{TE}} + \frac{P_{diss}^{TM}}{2P_{rad}^{TM}} \\ &= \frac{\operatorname{Re}(\eta_c)}{2\eta} \left[\frac{1}{\operatorname{Re}(Z_{mn}^{TE})} + \frac{1}{\operatorname{Re}(Z_{mn}^{TM})} \right] \end{aligned} \quad (2.5.5)$$

As the Z_{nm} are independent of m , the D_n are also independent of m . Harrington defined the characteristic impedances outside the spherical conductor as

$$\begin{aligned} Z_{mn}^{TE} &= \frac{F_n(\beta r)}{jF'_n(\beta r)} \\ Z_{mn}^{TM} &= \frac{jF'_n(\beta r)}{F_n(\beta r)} \end{aligned} \quad (2.5.6)$$

where $F_n(\beta r)$ is defined in 2.4.2. Using 2.5.6 in 2.5.5 the result is

$$\begin{aligned} D_n(\beta R) &= \frac{\text{Re}(\eta_n)}{2\eta} [|F'_n(\beta R)|^2 + |F_n(\beta R)|^2] \\ &= \frac{\text{Re}(\eta_n)}{2\eta} [|\mu_n|^2 - 2] \end{aligned} \quad (2.5.7)$$

where $\mu_n(\beta R)$ is defined in 2.4.6. Harrington defines the total dissipation for an antenna with equal TE and TM excitation as

$$D = \frac{P_{diss}}{P_{rad}} = \frac{\sum_{m,n} \text{Re}(P_{mn}) D_n}{\sum_{m,n} \text{Re}(P_{mn})} \quad (2.5.8)$$

where P_{mn} is the power in both the TE and TM modes. As $|\mu_{n+1}|^2 > |\mu_n|^2$ it can be seen from 2.5.7 that $D_{n+1} > D_n$. Using this and 2.5.8 it is clear that the lowest dissipation occurs when only the lowest order mode is excited. Thus the minimum dissipation is equal to D_1 . The percentage efficiency is given by

$$eff = \frac{100}{1 + D_1} \quad (2.5.9)$$

The maximum percentage efficiency versus antenna size is shown in figure 2.8 for lossy antennas constructed of aluminium and of copper. As the approximations in this derivation are only valid for electrically small antennas, the values become unrealistic for $kr > 1$.

From figure 2.8 it can be seen that as the antenna size is reduced there is a significant decrease in the achievable radiation efficiency.

As many electrically small antennas are not resonant in themselves, they need some sort of matching network. Smith (11) showed how the large Q of electrically small antennas negatively impacts the efficiency of an antenna combined with a

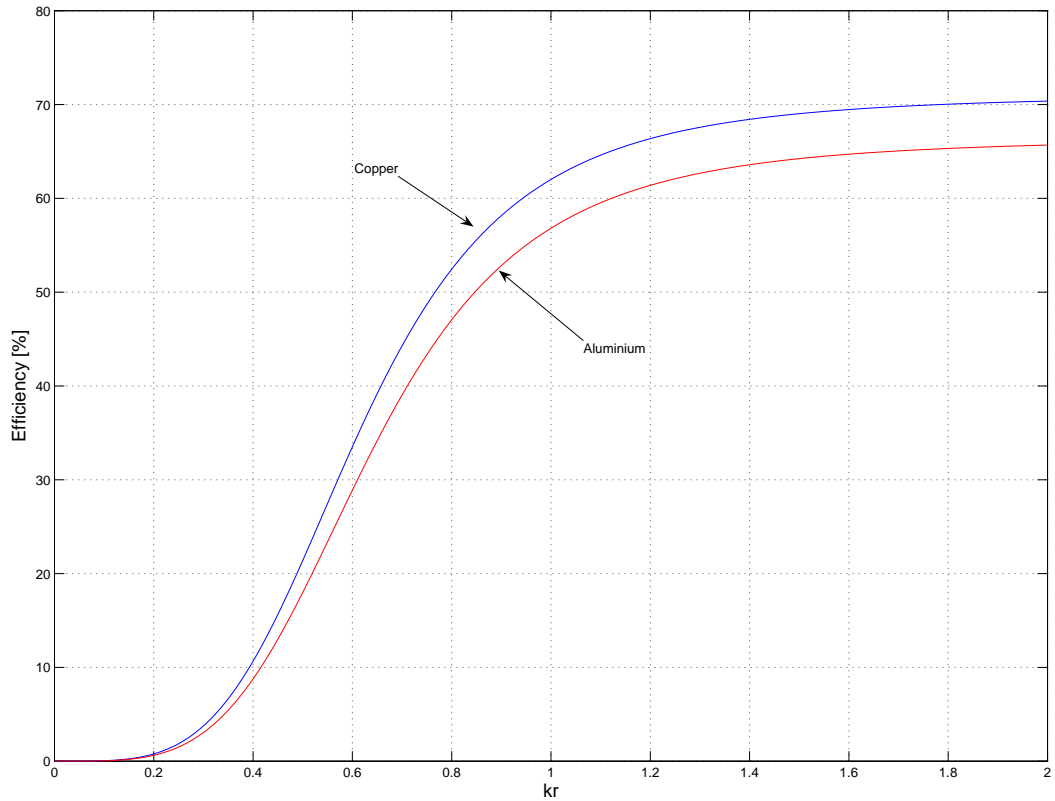


Figure 2.8: Percentage efficiency for aluminium and copper antennas versus relative size. The approximation becomes invalid for $kr > 1$.

matching network. When an antenna is combined with a matching network to optimize the transfer of energy from the antenna to the receiver or from the transmitter to the antenna the system efficiency is a combination of the antenna and matching network's efficiency. For a transmitting antenna

$$\eta_s = \frac{P_r}{P_{in}} = \eta_m \eta_a \quad (2.5.10)$$

where P_{in} is the average power supplied to the system, P_r is the average power radiated, η_m is the efficiency of the matching network and η_a is the efficiency of the

antenna.

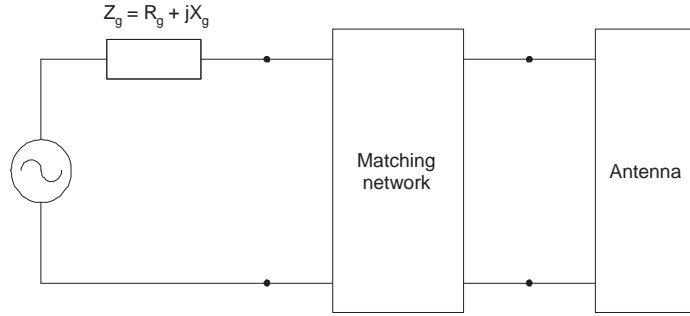


Figure 2.9: Schematic of antenna with matching network.

Figure 2.9 shows an system consisting of a matching network connecting an antenna to a generator with a source impedance of $R_g + jX_g$. The radiation efficiency and Q of the antenna are given by

$$\eta_a = \frac{P_r}{P_a}, \quad Q_a = \frac{2\omega U_a}{P_a}. \quad (2.5.11)$$

Each element in the matching network, just like the antenna itself, either stores an average electric or average magnetic energy at a given frequency. Elements storing the same type of energy as the antenna are described by Q_i and elements storing the opposite form by Q'_i . This yields

$$Q_i = \frac{2\omega U_i}{P_i} \quad Q'_i = \frac{2\omega U'_i}{P'_i}. \quad (2.5.12)$$

The input of the matching network is conjugate matched to the source to assure maximum power P_{in} is transferred from the source to the matching network. Under a conjugate match the power dissipated in R_g is equal to P_{in} . The Q for the source impedance is then

$$Q_g = \frac{|X_g|}{R_g} = \frac{2\omega U_g}{P_{in}} \quad (2.5.13)$$

where U_g is the average reactive energy stored in the source impedance. By applying conservation of energy the following equations for the circuit is produced

$$P_{in} = P_a + \sum_{i=1}^n P_i + \sum_{i=1}^m P'_i \quad (2.5.14)$$

$$\sum_{i=1}^m U'_i = U_a + \sum_{i=1}^n U_i \pm U_g \quad (2.5.15)$$

with n and m the numbers of each element of the matching network. If the reactive energy stored in Z_g is of the same form as that of the antenna, the sign of the last term in 2.5.15 is $+$ else it is $-$. If all the elements of the same type in the matching network have the same Q then 2.5.14 and 2.5.15 become

$$P_{in} = P_a + \frac{2\omega}{Q} \sum_{i=1}^n U_i + \sum_{i=1}^m P'_i \quad (2.5.16)$$

$$Q' \sum_{i=1}^m P'_i = Q_a P_a + 2\omega \sum_{i=1}^n U_i \pm Q_g P_{in}. \quad (2.5.17)$$

By combining 2.5.16 and 2.5.17 the efficiency of the matching network is

$$\eta_m = \frac{P_a}{P_{in}} = \frac{1 \mp \frac{Q_g}{Q'} - \left(\frac{1}{Q} + \frac{1}{Q'}\right) \left(2\omega \sum_{i=1}^n \frac{U_i}{P_{in}}\right)}{1 + \frac{Q_a}{Q'}}. \quad (2.5.18)$$

As the source impedance is mostly resistive Q_g will be much less than the Q of the elements in the matching network. This means that $\frac{Q_g}{Q'} \approx 0$. With this in mind it is clear from 2.5.18 that a maximum efficiency is achieved when all the elements of the matching network only store energy in the opposite form as the antenna and $U_i = 0$. This is because there is no exchange of energy between elements of the matching network which produces additional loss. Thus the maximum efficiency of the combined system becomes

$$\eta_s = \eta_a \eta_m = \frac{\eta_a}{1 + \frac{Q_a}{Q'}}. \quad (2.5.19)$$

As the Q of an electrically small antenna is of the order of the Q of the matching network, it can be seen from 2.5.19 that the matching network has a substantially detrimental effect on the efficiency of an electrically small antenna combined with a matching network. As such, self-resonant structures should be preferred above structures that require additional matching.

Chapter 3

Electrically small antennas

3.1 Introduction

In the field of antennas, as in all other areas of engineering, miniaturization is a great area of interest. Much work has been done in this regard and many varying techniques for size reduction have been proposed. In this chapter various planar electrically small antennas that are commonly used and that have been proposed will be considered. With the theory developed in chapter 2 in mind these antennas are critically examined. Their operation with regards to their input impedance and their bandwidth performance are considered. In an attempt to gain better understanding into the working of electrically small antennas, all these antenna were simulated in FEKO which is a full wave, method of moments based electromagnetic solver.

3.2 Multi-element monopole antenna

The quarter-wave monopole is one of the the most simple antennas. It consists of a quarter wavelength long vertical wire fed above a ground plane as shown in figure 3.1. Because of its simple construction the monopole is one of the most commonly used antennas for mobile equipment.

Because of its simplicity and relatively small size the quarter-wave monopole is very widely used for television and radio transmissions. Until recently it was also widely used in cellular and cordless telephones.

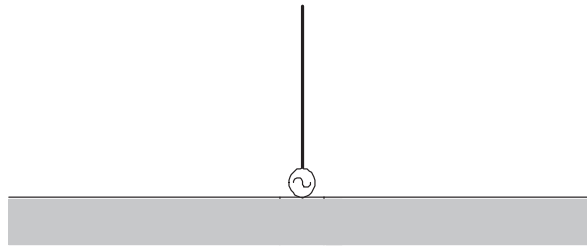


Figure 3.1: Quarter-wave monopole antenna

By folding a half-wave monopole as shown in figure 3.2 an quarter-wave antenna that more effectively utilizes the available space is created.

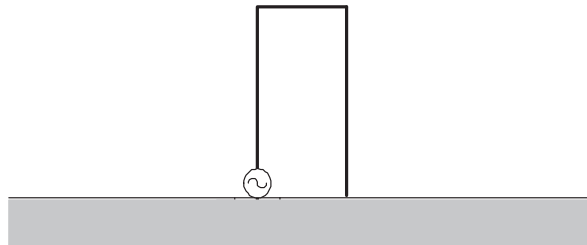


Figure 3.2: Folded monopole antenna

As such this folded monopole antenna has a much improved bandwidth as is shown in figure 3.3.

A very popular electrically small antenna is the top-loaded monopole antenna (13; 14). A top-loaded monopole is constructed by adding a capacitive top plate to the folded monopole antenna. It achieves resonance in a electrically small structure by balancing the electric field between the capacitive top-plate with the magnetic field around the monopole.

The addition of the capacitive plate significantly reduces the resonant frequency of the folded monopole antenna by increasing its effective length. As can be seen from figure 3.4 the resonant frequency for two antennas of equal height is nearly reduced by a factor of three. While the folded monopole antenna has a relative size of $kr = 1.335$, the top-loaded folded monopole has a relative size of $kr = 0.711$. As such it is an electrically small antenna.

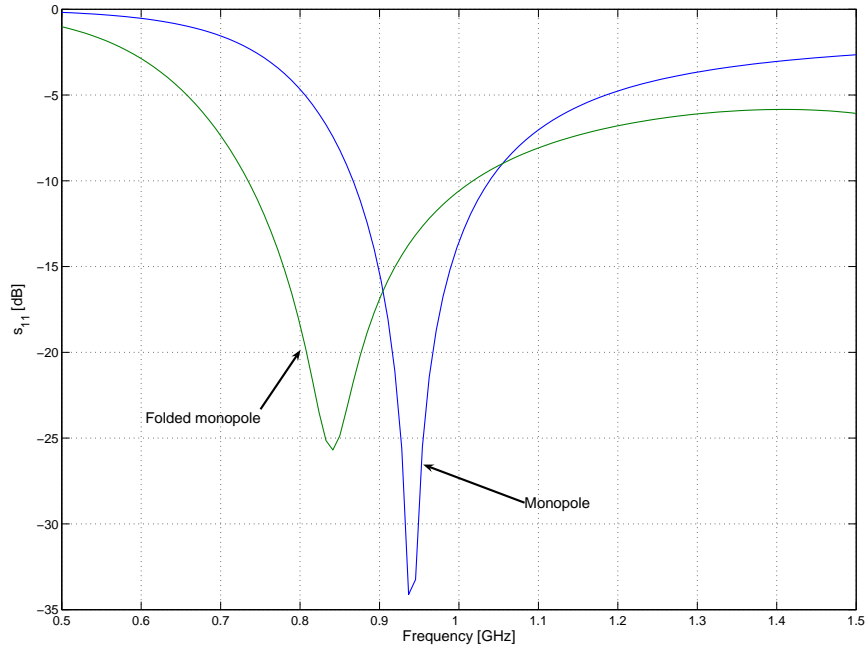


Figure 3.3: Simulated s_{11} of the quarter-wave and folded monopole antennas

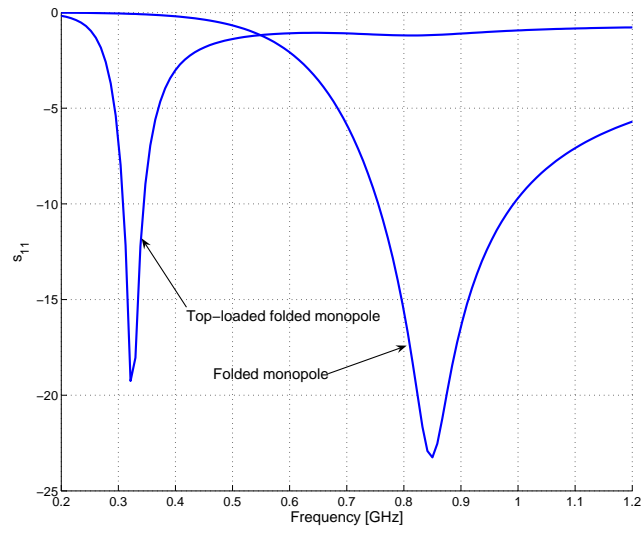


Figure 3.4: Simulated s_{11} for the folded monopole and top-loaded folded monopole antennas.

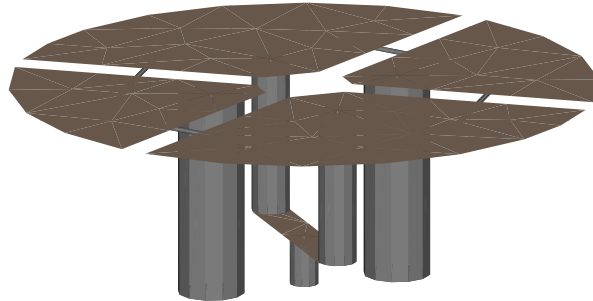


Figure 3.5: Goubau's broad-band multi-element monopole antenna.

The antenna proposed by Goubau (12) has long been seen as the benchmark against which all other electrically small antennas are measured. It consists of four top-loaded interconnected monopoles. In (12) Goubau relates the increased input impedance of a multi-element monopole antenna over a single monopole to the number of monopoles in the antenna. It is shown that, when only one of the multiple monopoles are fed the input current is given by

$$I = \frac{VY}{N^2} \quad (3.2.1)$$

It can be seen from 3.2.1 that the effective radiation resistance is increased by a factor N^2 . A simple example is the folded monopole which has a radiation resistance of approximately four times that of a single monopole of the same height.

Goubau then goes on to state that a broad-band multi-element antenna can be built by using a pair of thick monopoles with small capacitive plates along with a pair of thin monopoles with larger capacitive plates. The four monopoles are inductively interconnected at the top, just below the capacitive plates. This

antenna is shown in figure 3.5.

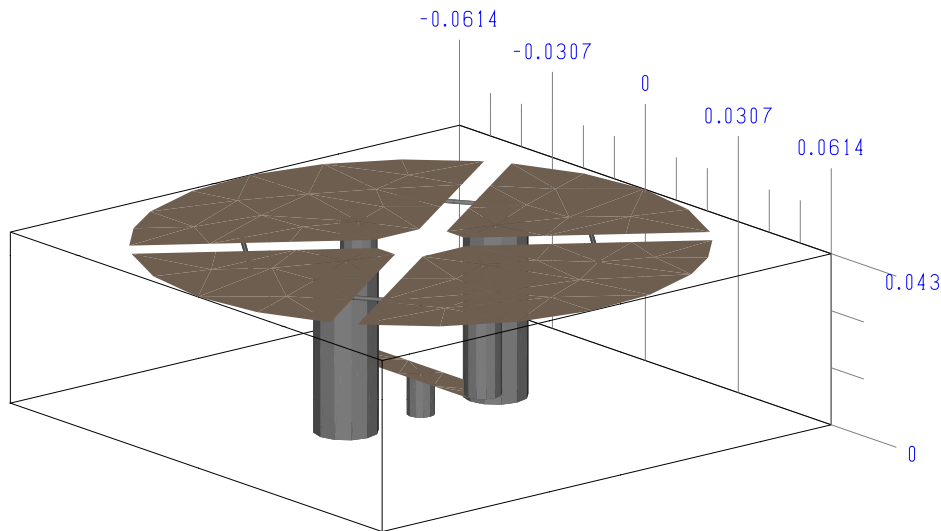


Figure 3.6: Dimensions of the simulated Goubau antenna in m.

In (12) Goubau only states the height of the antenna along with the radius of the capacitive plate. After various simulations in FEKO with varying monopole radii a frequency response similar to the one reported by Goubau was obtained. This antenna is shown in figure 3.6. Figure 3.7 shows the simulated s_{11} . The antenna has a half-power bandwidth of more than 75%. As $ka = 1.123$ at the center frequency, this antenna is only electrically small in the lower end of its frequency range.

In (12) Goubau does not attempt to explain the wide-band response of the antenna. As the total current path is much shorter than a wavelength, the currents on adjacent wires are relatively in-phase, but in opposite directions and thus their apparent current is less. Further, as the current is divided between four wires, the current density is much less. The lower apparent current and current density causes the magnetic energy stored in the antenna near-field to be much less. As was shown in chapter 2, less stored energy leads to lower Q and wider bandwidth. As the Goubau antenna is a complex structure, it has not become widely used, but it still remains an interesting antenna for the wide-band response it achieves in such a small structure.

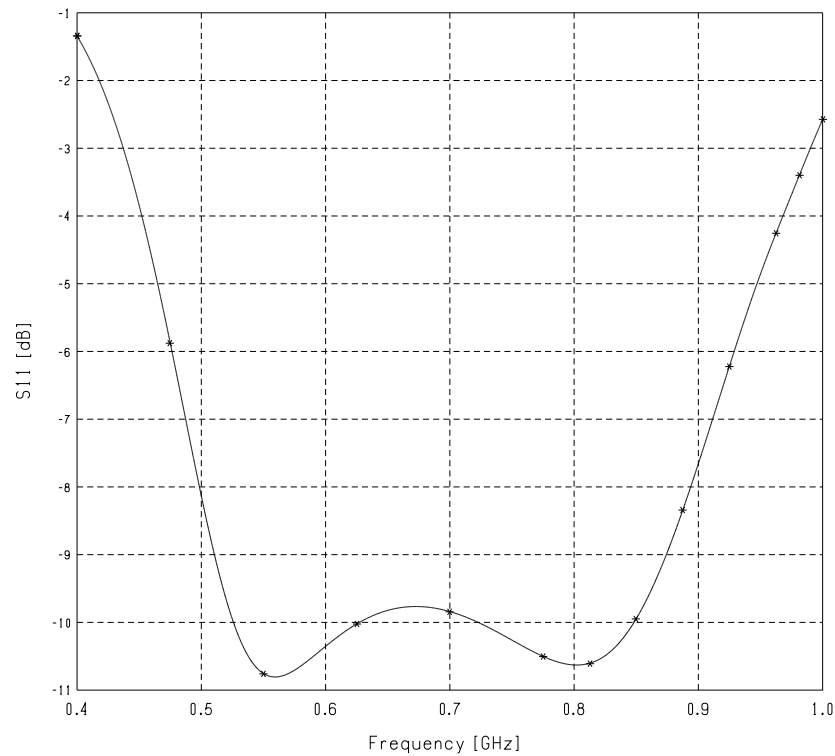


Figure 3.7: Simulated s_{11} of the Goubau antenna.

3.3 Loop fed spiral wire antenna

Physically folding or spiraling wire antennas is a simple way of reducing their size. Choo and Ling (15) proposed the electrically small planar wire antenna of figure 3.8. This antenna is planar in a plane perpendicular to the ground plane. The radiating structure is a rectangular spiraled wire while the feed is a rectangular wire loop that couples inductively to the radiating structure. The spiraling of the radiating structure decreases its size while the inductive coupling at the feed increases the input resistance of the antenna.

Choo and Ling used the Pareto genetic algorithm (16) to optimize the antenna for best bandwidth, highest efficiency and smallest size. An antenna with the dimensions of figure 3.9 has a relative size of $kr = 0.36$. This antenna was simulated and its s_{11} is shown in figure 3.10. It shows a half-power bandwidth of 1.5%.

To create a truly planar antenna, Choo and Ling translated this design into a

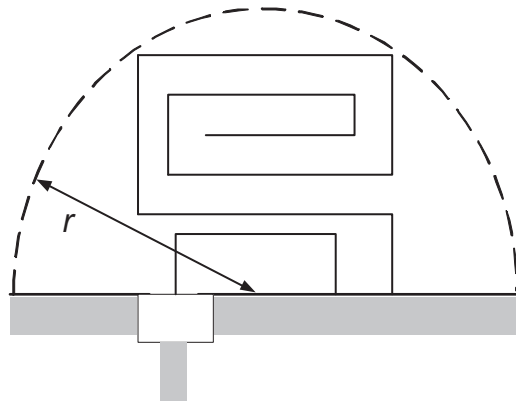


Figure 3.8: Design of the electrically small planar wire antenna.

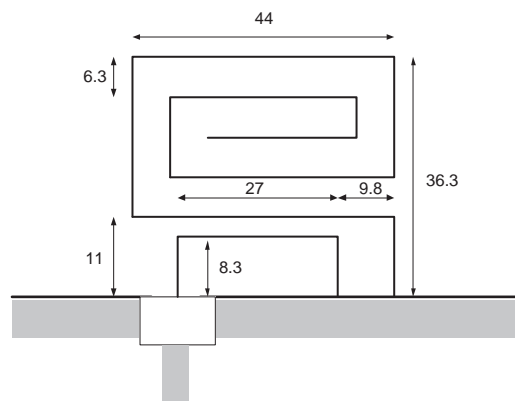


Figure 3.9: Dimensions of antenna A in mm.

printed antenna by using 2mm wide microstrip lines on 0.8 mm FR-4 substrate. This antenna is truly planar in the sense that the whole antenna is in one plane: the ground plane. This produced a frequency shift from 400 MHz to 355 MHz, but also a broader bandwidth. The efficiency also dropped substantially. Because of the high dielectric constant ($\epsilon_r = 4.2$) the antenna is much smaller than the wire antenna which is in free-space.

Choo and Ling proposed a lumped element circuit model to explain the operation of the inductively coupled feed. This circuit model is shown in figure 3.11

The inductive coupling of the feed is modeled by a transformer. From the circuit model of figure 3.11 the input impedance of the antenna is given by

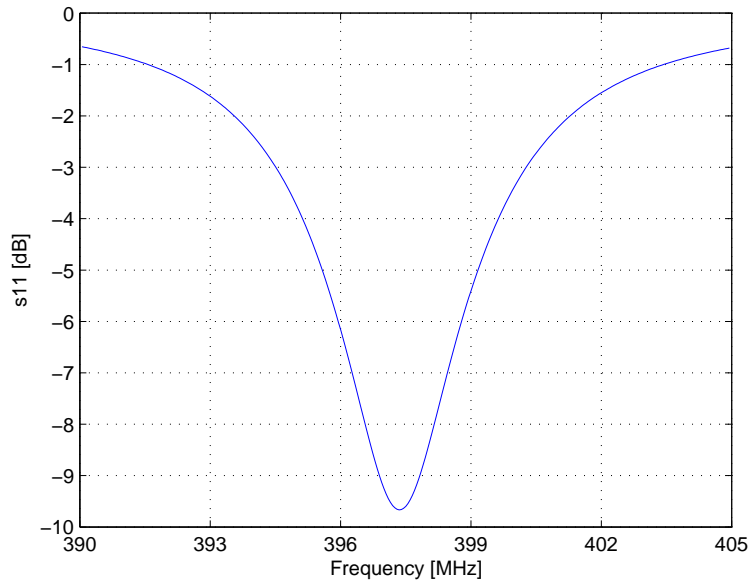


Figure 3.10: Simulated s_{11} for antenna A of figure 3.9 .

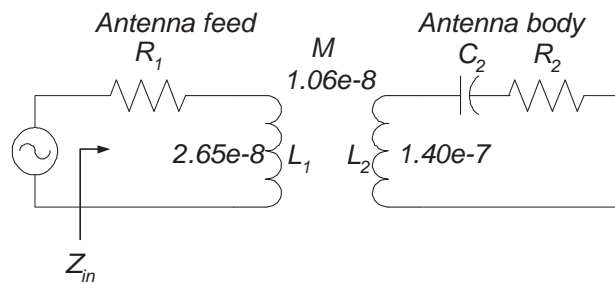


Figure 3.11: Lumped element circuit model.

$$Z_{in} = Z_{feed} + \frac{\omega^2 M^2}{Z_{body}} \quad (3.3.1)$$

This clearly shows that the inductively coupled feed serves to invert and amplify the small input resistance of the antenna body. Figure 3.12 shows that the input reactance of the antenna is equal to zero at two points near the operating frequency. This double resonance increases the bandwidth of the antenna.

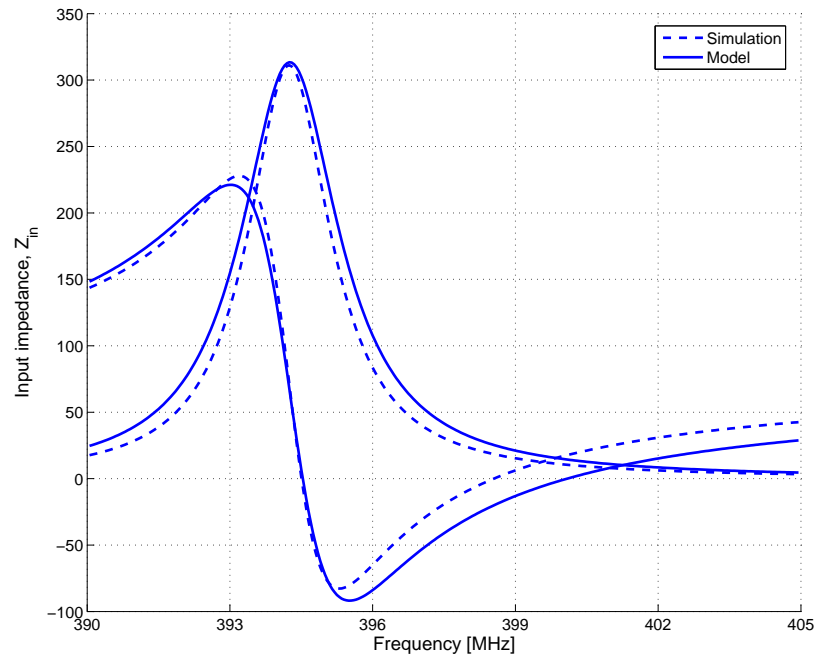


Figure 3.12: Input impedance of the lumped element model and the simulated response.

By combining the size reduction of the spiraling of the radiating wire with the impedance transformation of the inductively coupled feed, Choo and Ling produced an antenna that is electrically small and self-resonant.

3.4 Dielectrically loaded patch antenna

The wavelength in a dielectric medium is dependent on the dielectric constant of the medium. Increasing the dielectric loading of the substrate of a patch antenna reduces the resonant size of the patch. As such dielectric loading is a simple way of minimizing an patch antenna.

From Balanis (17) the resonant radius a of a circular patch antenna for a given resonant frequency f_r and a given substrate with dielectric constant ϵ_r and height h is given by

$$a = \frac{F}{\left\{1 + \frac{2h}{\pi\epsilon_r F} \left[\ln \left(\frac{\pi F}{2h} \right) + 1.7726 \right] \right\}^{\frac{1}{2}}} \quad (3.4.1)$$

where $F = \frac{8.791 \times 10^9}{f_r \sqrt{\epsilon_r}}$ and h is in centimeters. Figure 3.13 shows how dielectrically loading the substrate reduces the size of the patch antenna. But this reduction comes at the cost of bandwidth. As shown in figure 3.14 dielectric loading to decrease the size of a patch antenna reduces the bandwidth. This is because the higher dielectric constant leads to more stored energy relative to the radiated power. This results in a higher Q-factor and a lower bandwidth. While the circular patch antenna was taken as an example here the same applies to all types of patch antennas. It is clear that, when the required bandwidth for patch antenna is relatively small, dielectric loading is a worthwhile consideration, but, when bandwidth is an important factor in a design, care should be taken in this regard.

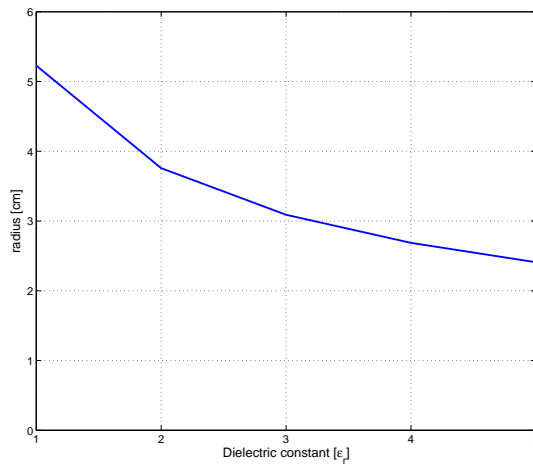


Figure 3.13: Circular patch size against ϵ_r for $f_r = 1.6GHz$ and $h = 1.588mm$.

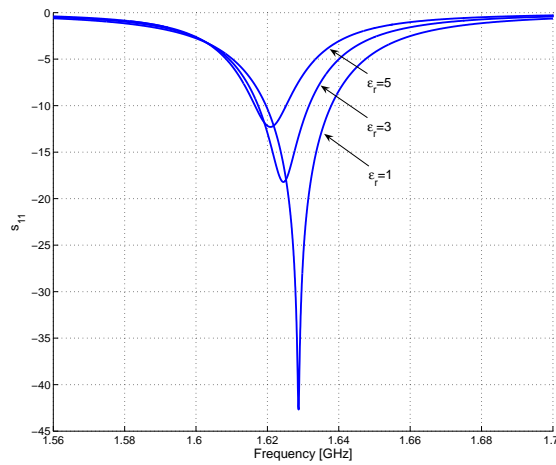


Figure 3.14: Simulated s_{11} for circular patch antennas with various values of ϵ_r and $f_r = 1.6GHz$ and $h = 1.588mm$.

3.5 Shorted probe fed microstrip antenna

Recently Waterhouse (18; 19; 20; 21) proposed another electrically small microstrip patch antenna. The antenna consists of a microstrip patch that is pin-fed and has one or more shorting posts. The largest reduction in size is obtained when a single shorting post is used. Figure 3.15 shows the layout of such an antenna.

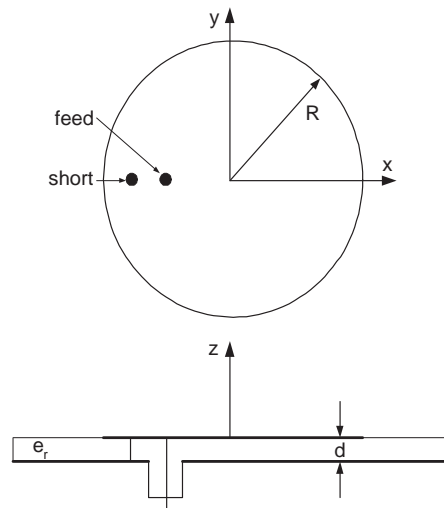


Figure 3.15: Schematic of probe-fed patch with shorting post.

Waterhouse explains the operation of this type of antenna through simple circuit theory in (20). The effect of the shorting post is represented by a LC circuit parallel to the RLC circuit used to describe the working of a probe fed patch antenna. The closer the shorting post is placed to the feed probe, the greater the effect of the capacitance between them. The parallel combination of this capacitive effect and the inductive effect of the probe fed patch below resonance results in a resonant antenna with a significant reduction in overall size. The antenna of figure 3.15 was simulated with $R = 10.65mm$ and $d = 10mm$. At the simulated center frequency of $1.9GHz$ this is equal to an effective size of $kr = 0.58$. The simulated s_{11} for this antenna is shown in figure 3.16. The antenna has a half power bandwidth of 19.2%.

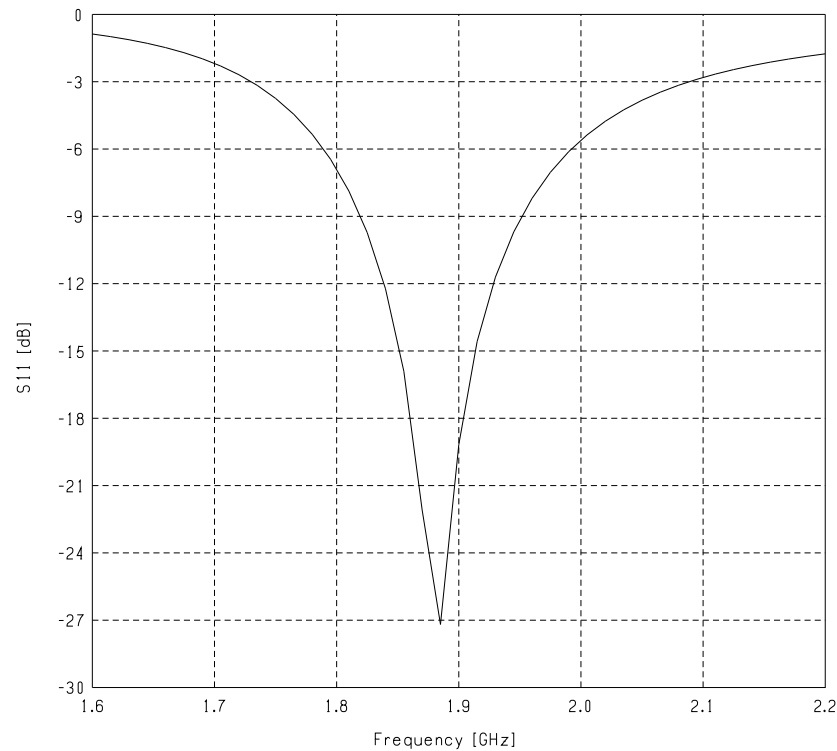


Figure 3.16: Simulated s_{11} of the probe-fed patch with shorting post.

3.6 Planar inverted-F antenna

The Planar Inverted-F Antenna (PIFA) is widely used in applications where an electrically small planar antenna is needed. In recent years it has come to surpass the monopole antenna as the antenna of choice for mobile communications equipment such as cellular and cordless telephones. Because of its compact planar design the antenna can be incorporated within the device unlike the monopole antenna which needs to be placed external to the device.

Figure 3.17 (from James (22)) shows a open-circuit half-wave microstrip patch antenna operating in the dominant mode. The patch antenna has a zero-voltage line at its center. If this line is short-circuited to ground and half of the structure is removed, the field pattern in the resulting quarter-wave patch remains unchanged. A planar inverted-F antenna is constructed by shorting the zero potential plane of a microstrip antenna fed in the dominant mode as shown in figure 3.17. The result

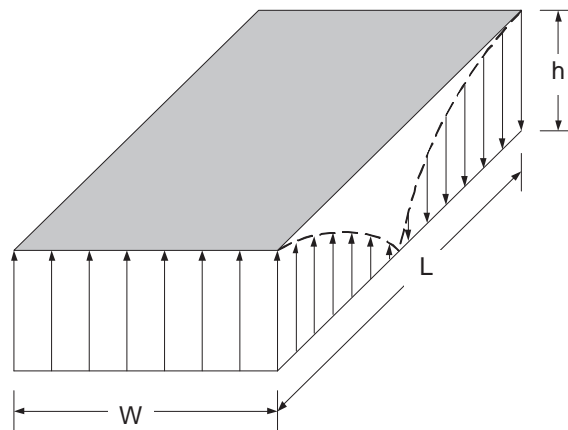


Figure 3.17: E-field pattern for half-wave microstrip patch antenna.

is a resonant planar structure that is only a quarter-wavelength in size.

Simulations show that the input impedance of the PIFA at resonance is in the order of twice that of the patch antenna. This results in the power radiated by the PIFA for the same edge voltage being half that of the patch. As the PIFA is half the size of the patch antenna, its stored energy is also halved. This results in both antennas having similar Q-factors and bandwidths. Figure 3.18 shows the simulated s_{11} for a $\frac{\lambda}{2}$ patch and its corresponding $\frac{\lambda}{4}$ PIFA. It is clear that the bandwidths are very similar. This size reduction without excessive loss of bandwidth makes the planar inverted-F a very popular antenna. As such much work has been done on this geometry. Many variations on the standard PIFA have been proposed and implemented. Salonen (23) proposed a PIFA with a U-shaped slot for dual-band operation. Hwang (24) proposed further size reduction by loading the PIFA with high permittivity material. Li (25) proposed a broadband triangular PIFA, while Row (26) incorporated a V-shaped slot to realize a dual-frequency triangular PIFA. Rowell (27) found that capacitively loading the PIFA reduces its size further by a factor of more than two.

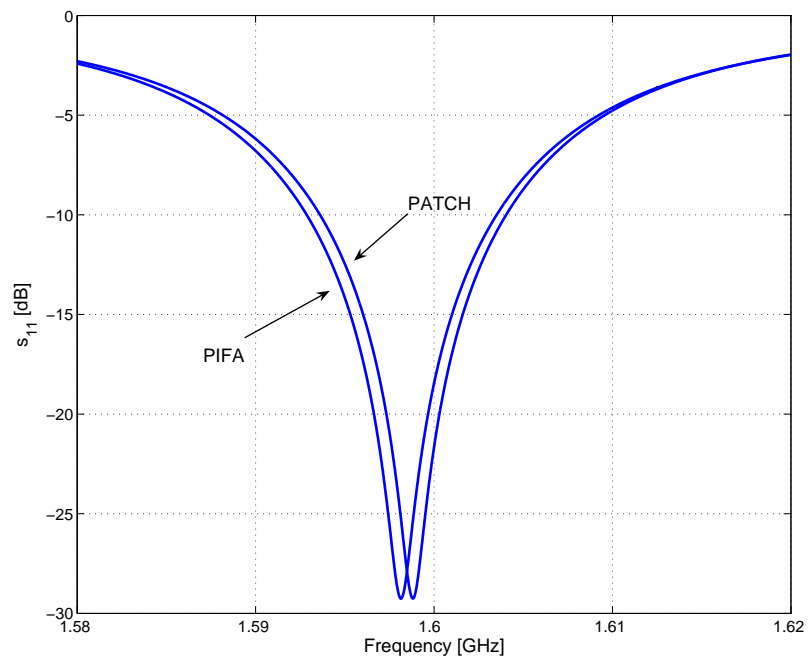


Figure 3.18: Simulated s_{11} for the $\frac{\lambda}{2}$ patch and the $\frac{\lambda}{4}$ PIFA .

Chapter 4

Design of a sequentially rotated PIFA for circular polarization

4.1 Introduction

This chapter details the conceptual design of the antenna element, highlighting all aspects of the design process. Every design choice is clearly investigated and motivated.

4.2 Specifications

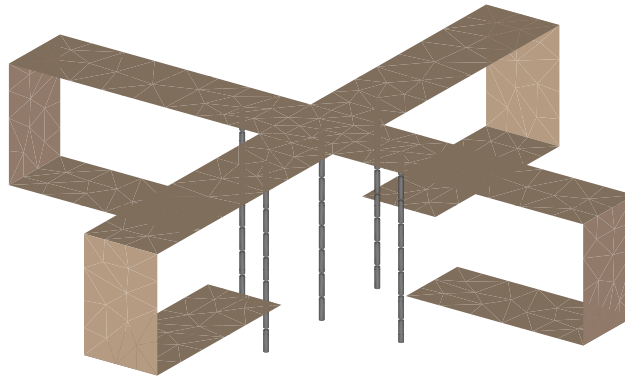
The goal was to design an electrically small patch-type structure to be used as an element in a beam steering array. The intended use is in a circularly polarized array which is required to scan as low as possible in elevation. The required receive band is 1525-1559 MHz and the transmit band 1626-1661 MHz. As there is a bandwidth limitation on electrically small antennas, separate receive and transmit elements are considered to reduce the bandwidth requirement from 8.5% to 2.2%.

4.3 Proposed design

A set of four sequentially rotated, sequentially fed, folded Planar Inverted-F Antennas (PIFA's) in a cross formation, as shown in figure 4.1 is proposed. The four antennas are sequentially rotated and fed to achieve the circular polarization. They

Table 4.1: Antenna design specifications

Specification	Symbol	Value
Receive band	RX	1525-1559 MHz
Transmit band	TX	1626-1661 MHz
Receive center frequency	f_0^{RX}	1542 MHz
Transmit center frequency	f_0^{TX}	1643 MHz

**Figure 4.1:** Final design.

are placed in a cross formation and all share the same shorting pin, to minimize the space used. As a PIFA is a quarter-wave structure, each of the antennas has to be folded for the whole cross structure to be smaller than a quarter wavelength.

4.4 Effect of the shorting pin as compared to a shorting plate

As stated by Sanad (28) it is much easier to manufacture a shorting pin between the patch and ground than shorting the edge of the PIFA with a plate to ground, except in the special case of the patch being on the end of the substrate. As this is not the case here, a single shorting pin in the center of the cross is used to short the edges of all four PIFA's. By co-locating the shortened edges of all four PIFA's, the

need for separate shorts is removed. Simulations showed that the effect of replacing the shorting plate with a shorting pin does not negatively effect the performance of the antenna.

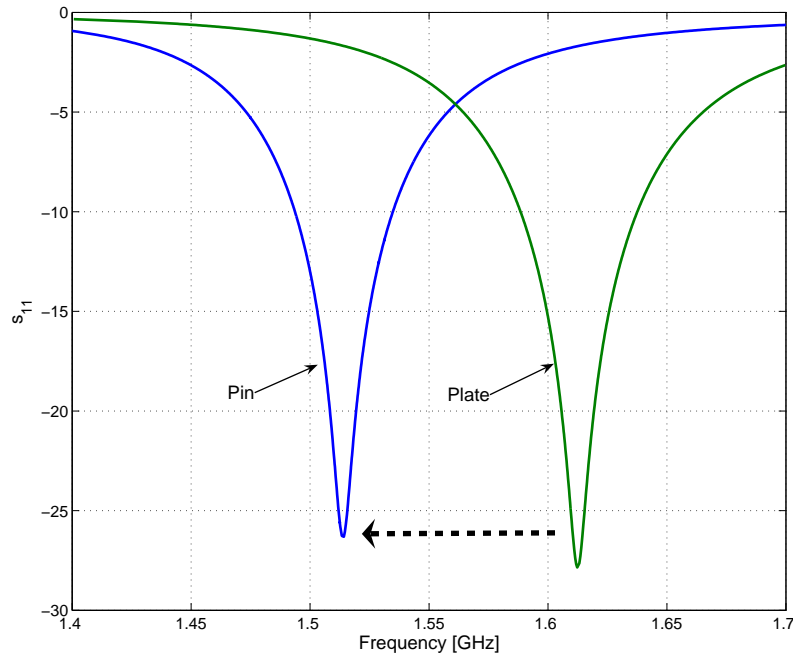


Figure 4.2: Simulated s_{11} of the pin-shortened and plate-shortened PIFA showing the reduction in resonant frequency.

As there is only one pin, it adds very little shunt capacitance and thus has a mostly inductive effect caused by the series inductance of the pin to ground. As can be seen from figure 4.2, this inductive effect decreases the resonant frequency of each PIFA. This further reduces the size without effecting the performance.

As the short at the edge of each of the four PIFA's terminates its surface current and the resulting fields, the four PIFA can be constructed from one cross structure without one significantly influencing the others.

4.5 Effect of folding the antenna body

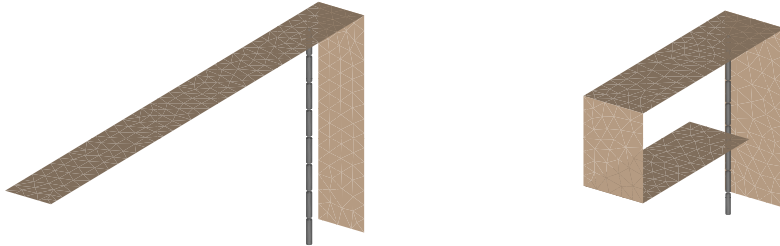


Figure 4.3: Unfolded and folded versions of the PIFA

The planar inverted-F antenna achieves resonance in a quarter-wave structure. To incorporate the four PIFA's in a cross structure within a quarter-wavelength it was necessary to fold each individual PIFA to halve its size in the horizontal plane. Folding the PIFA increased its resonant frequency and the body had to be lengthened slightly to compensate for this change. As was shown in Chapter 2 reducing the size of an antenna reduces the achievable bandwidth and as such folding the body has a detrimental effect on the bandwidth of a single PIFA as shown in figure 4.4. Simulations in FEKO showed that folding the PIFA reduces the $s_{11} < -15dB$ bandwidth from 2.83% for the unfolded PIFA to 1.75% for the folded case.

While this is a significant lose of bandwidth considering the required bandwidth of the element, the sacrifice had to be made to reach the desired size reduction.

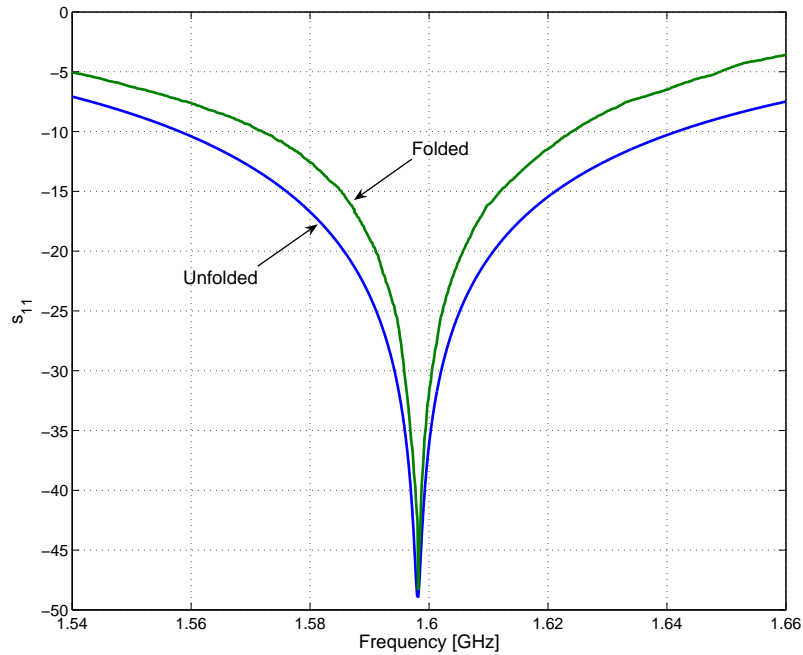


Figure 4.4: Simulated s_{11} for the unfolded and folded PIFA's.

4.6 Sequential rotation for circular polarization

Circular polarization is achieved by the arraying of the four PIFA's. The four elements are rotated around their common shorting pin and placed 90° apart as shown schematically in figure 4.5.

Each PIFA element is fed with a phase lagging its predecessor by 90° . If the amplitude of all four excitations are equal and the phasing is perfect, the vector addition of these four elements yields a rotating vector with a maximum size of twice that of a single element. This rotating field vector propagates a circularly polarized wave as is shown in figure 4.6.

Looking in the direction of propagation the wave is rotating clockwise and the polarization is thus said to be right-hand circular.

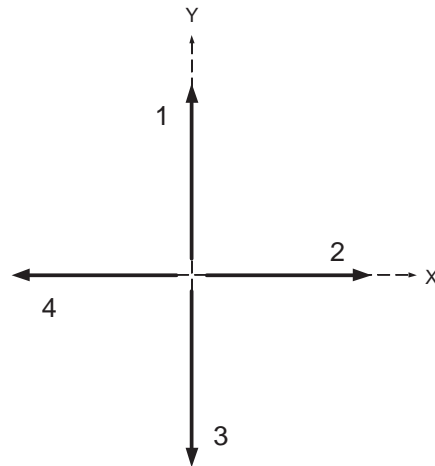


Figure 4.5: Sequential rotation of the four elements.

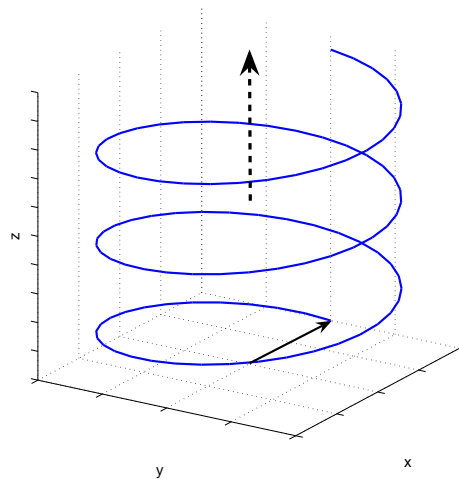


Figure 4.6: Rotating field vector.

4.7 Design of the feed network

The feed network is needed to:

feed all four arms of the antenna with equal power,

create the 90° phase shift between each sequential arm and

transform the input impedance of the antenna to 50Ω over the desired bandwidth.

The microstrip feed network was designed on 0.508mm Rogers RO4003C substrate with a relative permittivity of $\epsilon_r = 3.38$.

As can be seen from figure 4.7 the network consists of a quarter-wave transformer and a four way reactive power divider feeding four arms connected to each of the four PIFA's. The final feeding arms are 85Ω -lines to match to the inputs of the PIFA's. This means that the input to the four way power divider has an impedance of 21.25Ω . To transform this to 50Ω a quarter-wave transformer consisting of a quarter-wavelength long 32.6Ω -line, is used.

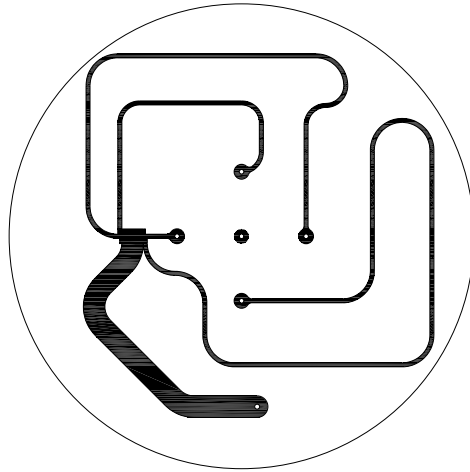


Figure 4.7: Layout of the feed network.

The 90° phase shift between sequential arms was obtained by making the electric length of each arm a quarter-wavelength longer than its predecessor. This resulted in the fourth and longest arm being three quarters of a wavelength long. As the whole antenna had to be smaller than a quarter of a free-space wave-length across, the arms of the feed network were bent to fit under the radiating structure. Care was taken to place the microstrip lines as far as possible from each other, to ensure that there would not be any coupling between closely located lines. A distance greater than three times the substrate height was maintained between all lines.

The feed network was designed in Microwave Office which has the ability to very accurately simulate microstrip networks. Figure 4.8 shows the relative gain from the input to the four feed arms. It can be seen clearly that the longer the arm, the greater the losses. This results in an unequal power division between the four radiating elements. This unequal power division diminishes the achievable axial ratio.

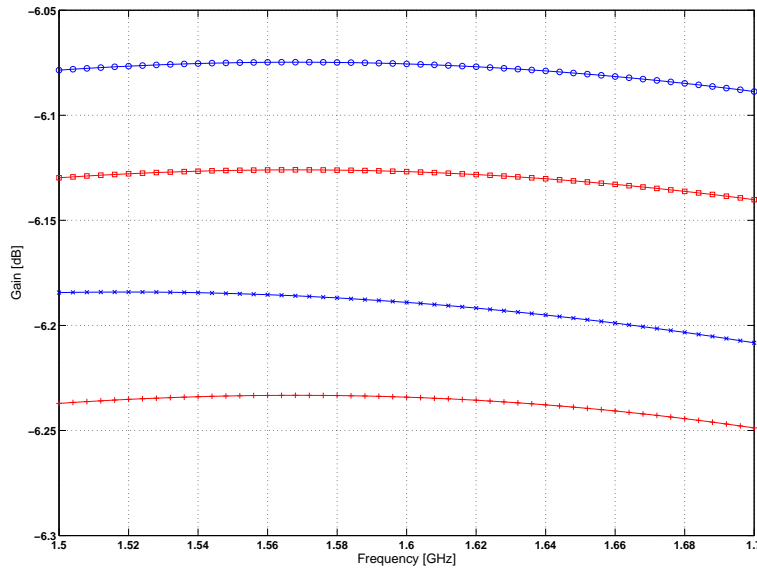


Figure 4.8: Simulated relative gain from input to each of the four arms of the feed network.

As shown by 4.7.1 the relative phase of each arm is dependent on the electric length of the arm and the electric length is proportional to the frequency. The longer the arm, the greater the change in phase over frequency. Figure 4.9 shows that the relative phase of the longer arms changes more rapidly with frequency than the shorter ones. As the axial ratio is dependent on the 90° phase shift between the sequential arms, this places a bandwidth limit on the axial ratio.

$$phase = \beta l = \frac{2\pi l}{\lambda} = \frac{2\pi fl}{c} \quad (4.7.1)$$

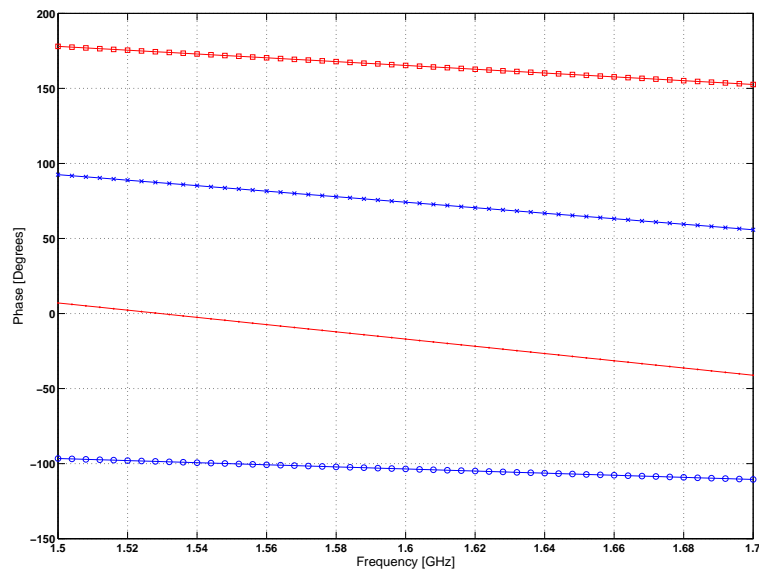


Figure 4.9: Simulated relative phase from input to each of the four arms of the feed network.

From the above it is clear that the feed network is not ideal and has a negative influence on the working of the antenna, resulting in reduced axial ratio and axial ratio bandwidth.

Chapter 5

Simulated and measured results of the sequentially rotated PIFA

5.1 Introduction

In this chapter the simulated and measured performance of the four-element PIFA array are presented. The construction of the antenna is described in detail and the simulated and measured results are compared and critically examined.

5.2 Simulation

The antenna was simulated in FEKO. FEKO is a full wave, Method of Moments based electromagnetic solver. Figure 5.1 shows the final FEKO-model. In the simulation each of the four ports of the antenna is fed with an ideal source. This meant that each arm received equal power and the correct phase to achieve the circular polarization over the whole band. This resulted in the simulations representing the antenna being fed by an ideal feed network.

Simulations of the far-field behavior of this ideally fed antenna showed that the four element array achieves good circularly polarized behavior. As can be seen from figure 5.2, a cross-polar discrimination of $15dB$ is achieved for angles as low as 70° .

The simulated s_{11} for one of the arms of the PIFA array is shown in figure 5.3. The bandwidth for $s_{11} < -15dB$ is equal to 1.27%.

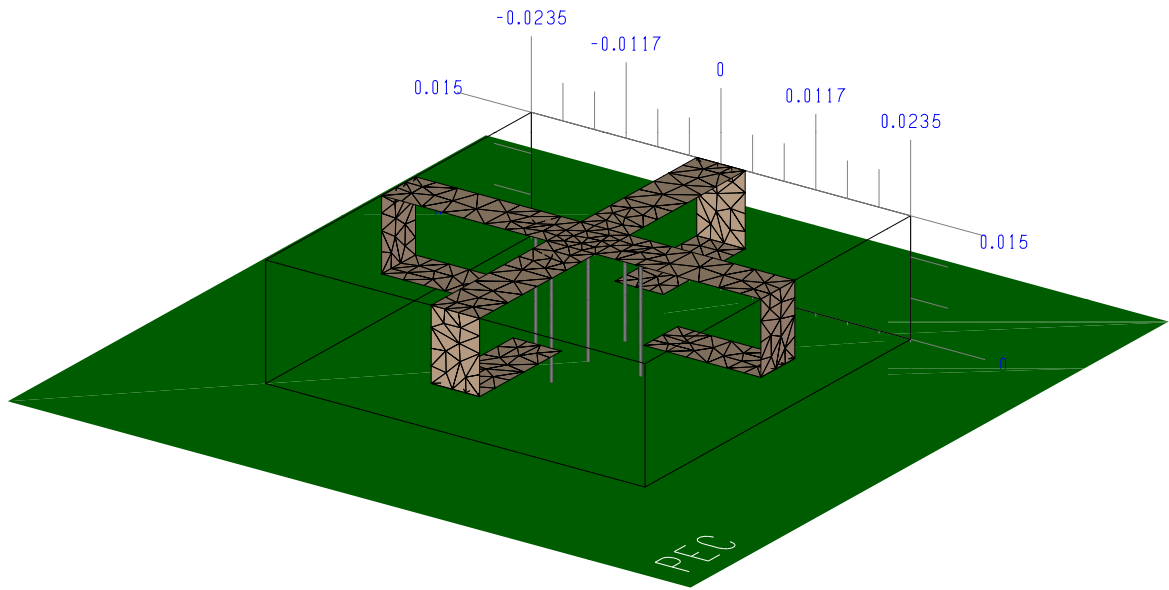


Figure 5.1: FEKO model of the antenna. Dimensions in m.

The S-parameters obtained through simulation were imported into MICROWAVE OFFICE and connected to the designed feed network. The resulting simulated s_{11} for the antenna connected to the feed network is shown in figure 5.4.

The feed network matches the four ports of the antenna to the 50Ω input port and in doing so significantly increased the simulated bandwidth for $s_{11} < -15dB$ from 1.27% for each single element to 3.53% for the combination of all four elements with the feed network.

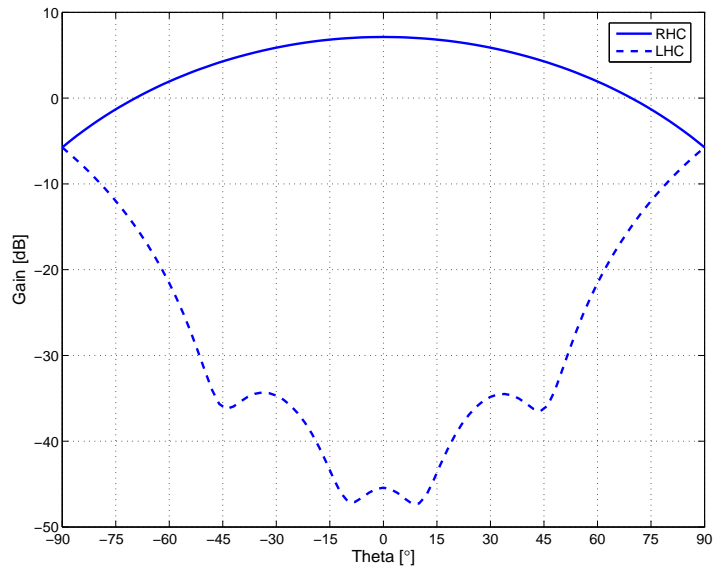


Figure 5.2: Simulated Right-hand (RHP) and Left-hand (LHP) polarized gain versus radiation angle..

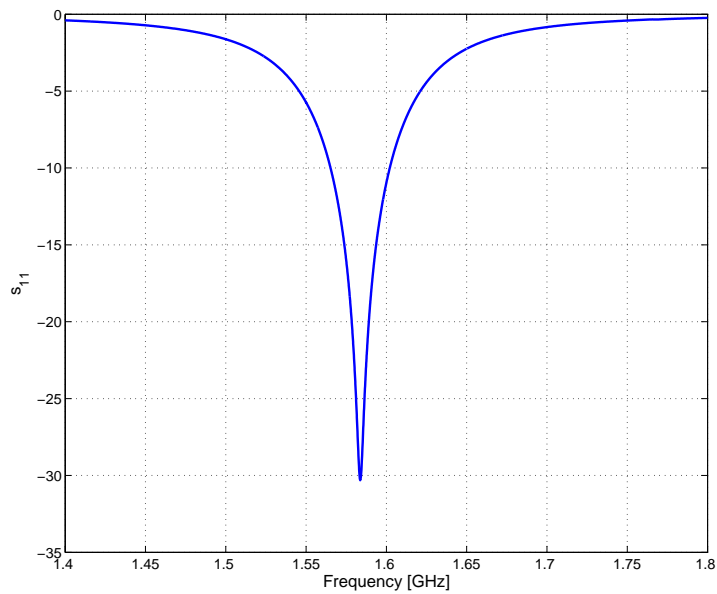


Figure 5.3: Simulated s_{11} for single PIFA element.

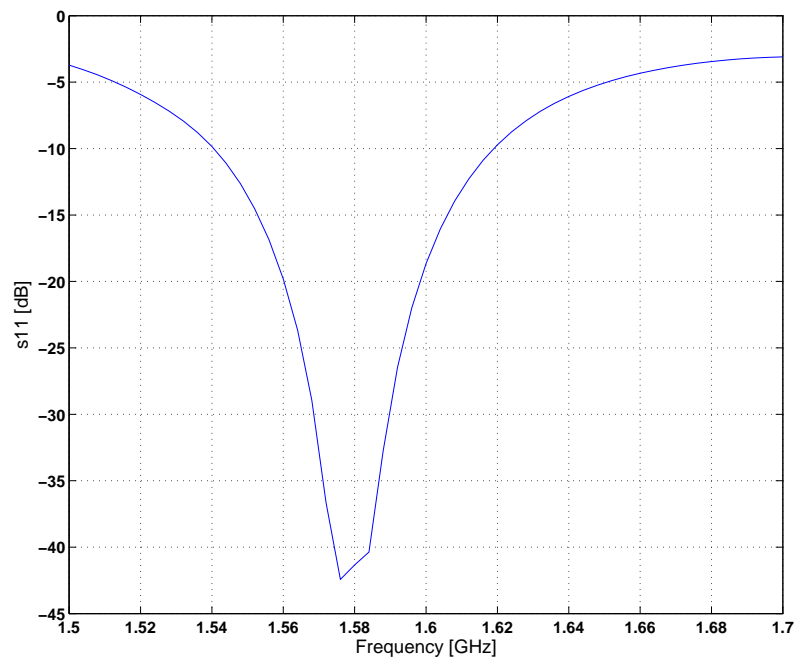


Figure 5.4: Simulated s_{11} of the antenna connected to the feed network.

5.3 Construction

The antenna was constructed by the University of Stellenbosch's Central Electronic Services. The cross-shaped radiating structure was etched out of 0.12mm copper plate and bent into the required shape. Layers of foam were used to keep the folded arms in place. The feed network was etched onto 0.508mm Rogers RO4003C substrate and hypodermic needles were used for the four feeding and one shorting pins. The needles were used because of their straightness and rigidity. The input to the feed network was fed by a SMA connector. The antenna was bolted onto a circular ground plane with radius $R = 300\text{mm}$.

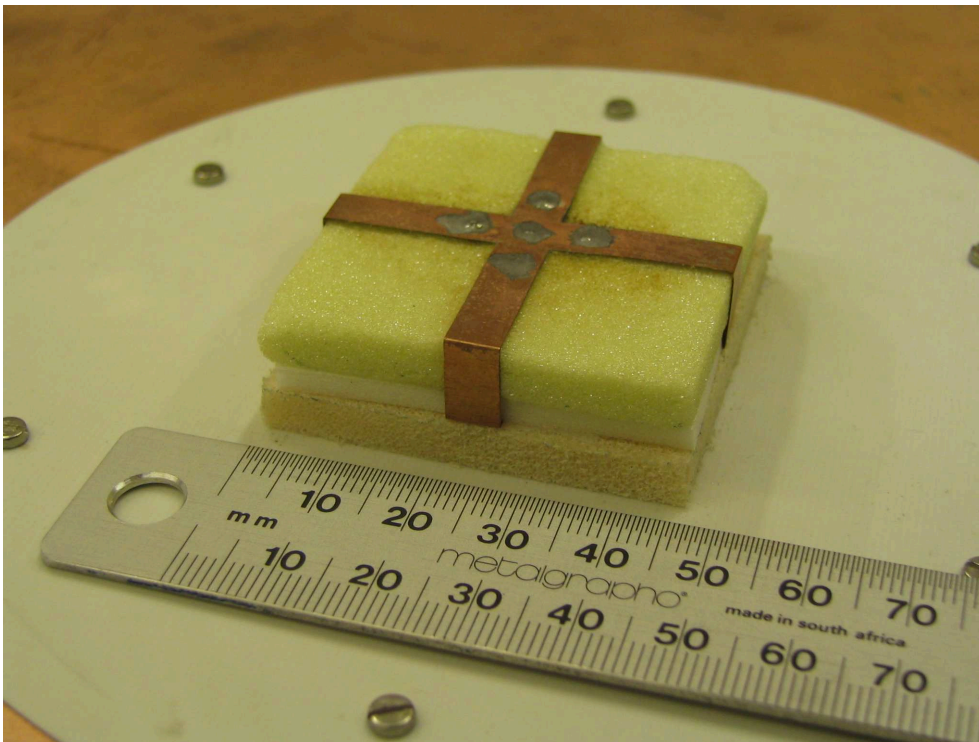


Figure 5.5: Final constructed antenna.



Figure 5.6: Antenna with conductive ground plane.

5.4 Measurement

The measurements were conducted at the University of Stellenbosch's High Frequency Laboratory in the anechoic chamber. The radiation pattern was measured using the three-antenna method. The antenna under test (AUT) and two reference antennas are used. Two log-periodic antennas were used as references. The s_{21} 's of all three possible combinations of two antennas are measured at bore sight and from these measurements the gain, at bore sight, of all three antennas can be calculated. To measure the radiation pattern one of the reference antennas was held static, first in the vertical and then in the horizontal position, while the AUT was rotated through 180° . These s_{21} measurements were taken at 1° intervals. From these measurements the right-hand and left-hand circular polarized gain could be calculated.

For far-field measurements a separation of $\frac{2D^2}{\lambda}$ between antennas is required. As a distance of $5m$ could be achieved between the measured antennas in the anechoic chamber, the measurements are an accurate representation of the far-field behavior of the antenna.

Figure 5.7 shows the measured s_{11} of the antenna. It shows a $s_{11} < -15dB$ bandwidth of 4.84%. Pattern measurements were taken at the center frequency of $1.541GHz$ and at the edge of the $-15dB$ -band at $1.562GHz$ which falls outside the required bandwidth of 2.2%.

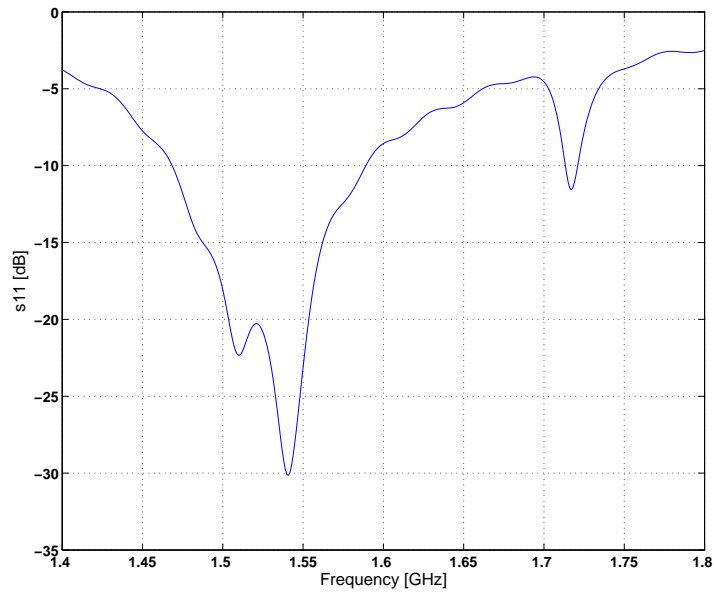


Figure 5.7: Measured s_{11} of the antenna input versus frequency.

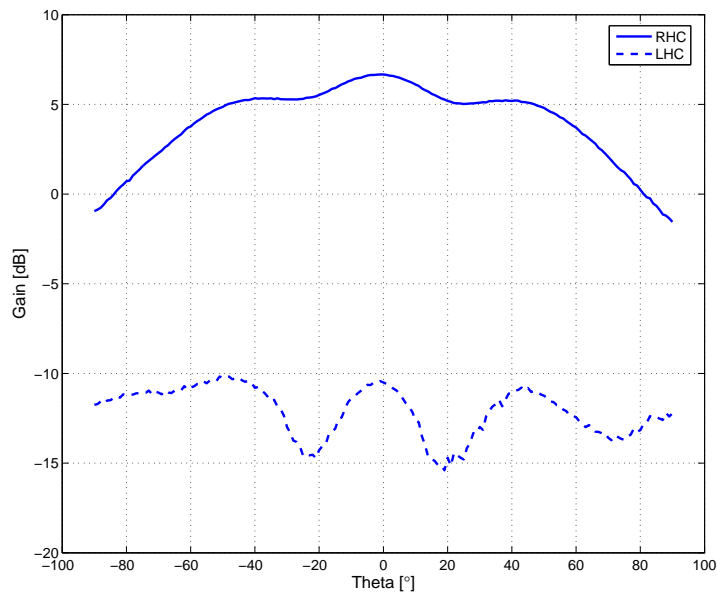


Figure 5.8: Measured Right-hand (RHP) and Left-hand (LHP) polarized gain versus radiation angle.

5.5 Results

In this section the measured and simulated results are compared and the differences are explained. Figure 5.9 shows the right-hand and left-hand polarized gain for both the simulation and the measurements at the center frequency. The simulations were conducted with an infinite ground plane and as the ground plane can not support a circularly polarized mode, the gain in the horizontal direction (at $\theta = 90^\circ$ and -90°) is linear as can be seen from figure 5.9, where the simulated right-hand and left-hand polarized gain is equal at $-6dB$ each. In contrast the finite ground plane used in the measurements does not have this effect and the right-hand and left-hand polarized gain differs by more than $10dB$ in the horizontal direction. Except for this difference the right-hand polarized gain for the simulated and measured response are in good agreement. A perfect feed network was used in the simulations as opposed to the imperfect feed network used in the measurements. This explains the much higher left-hand polarized gain measured. Figure 5.10 shows the right-hand and left-hand polarized gain for both the simulation and the measurements at the upper limit of the frequency band. The feed network is frequency sensitive and, at the higher frequency, the measured left-hand polarized gain is higher and degrades the performance of the antenna.

The anechoic chamber was designed for a measurement range of $2 - 18dB$ and this explains the measurement noise on the lower gain measurements.

Figure 5.11 shows the simulated and measured s_{11} of the antenna. A slight frequency shift occurred between simulation and measurement. This could be contributed to slight variations in the relative permittivity of the feed network substrate as well as the effect of the finite ground plane used in measurement.

The antenna was simulated in FEKO with a finite ground plane to confirm this. Figure 5.12 shows the effect of the finite versus the infinite ground plane.

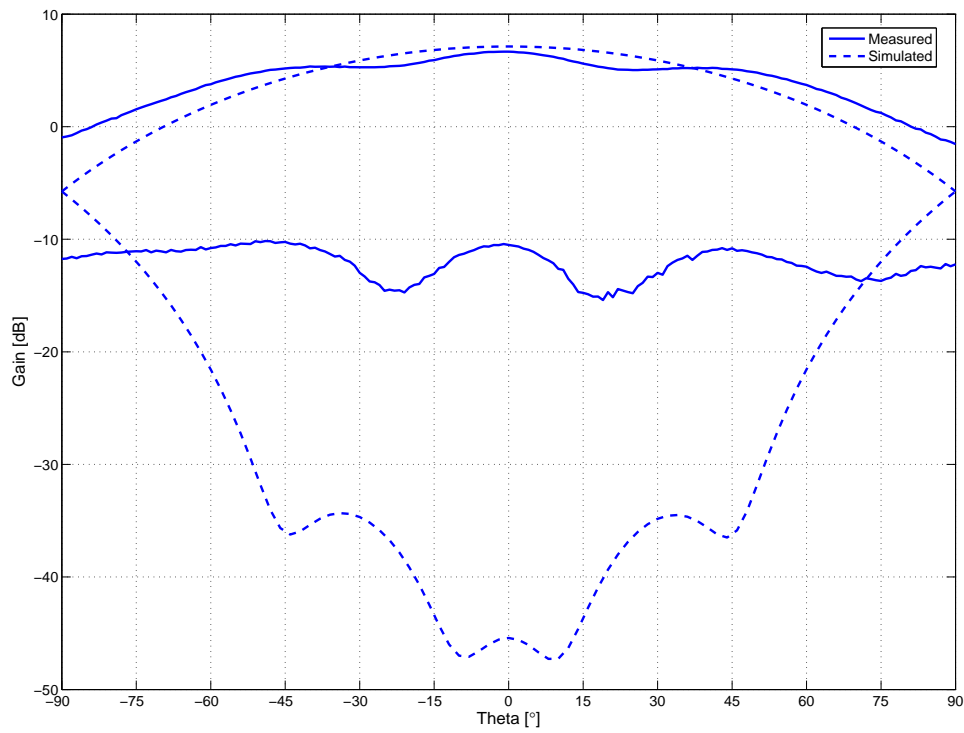


Figure 5.9: Measured and simulated right-hand and left-hand circularly polarized gain against theta at the center frequency of 1.541GHz .

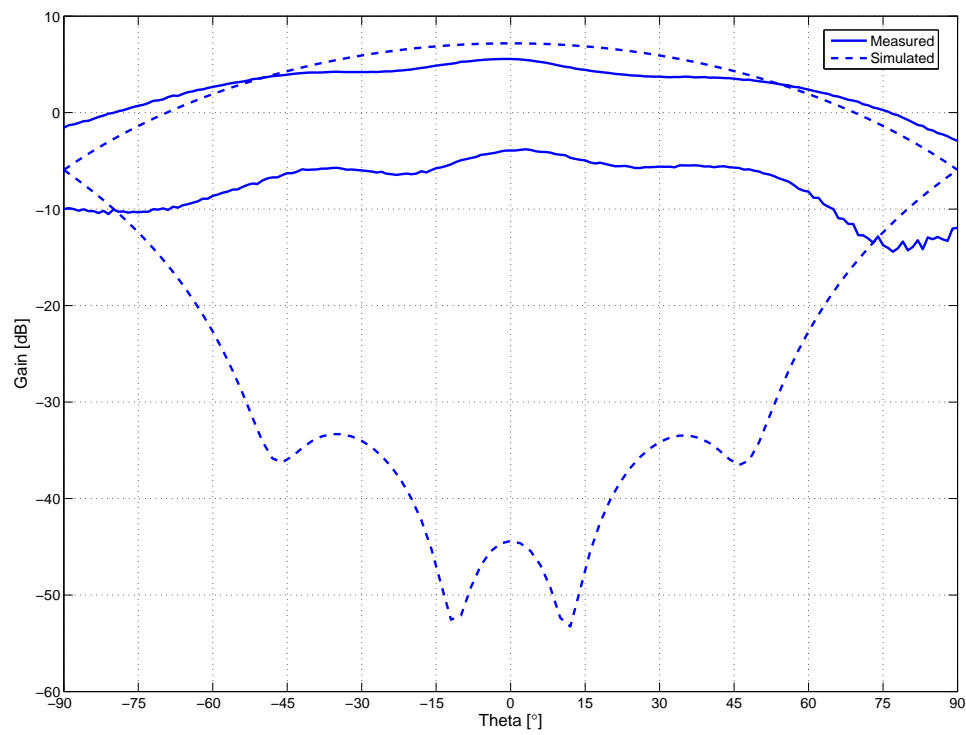


Figure 5.10: Measured and simulated right-hand and left-hand polarized gain against theta at the upper limit of the frequency band at $1.562GHz$.

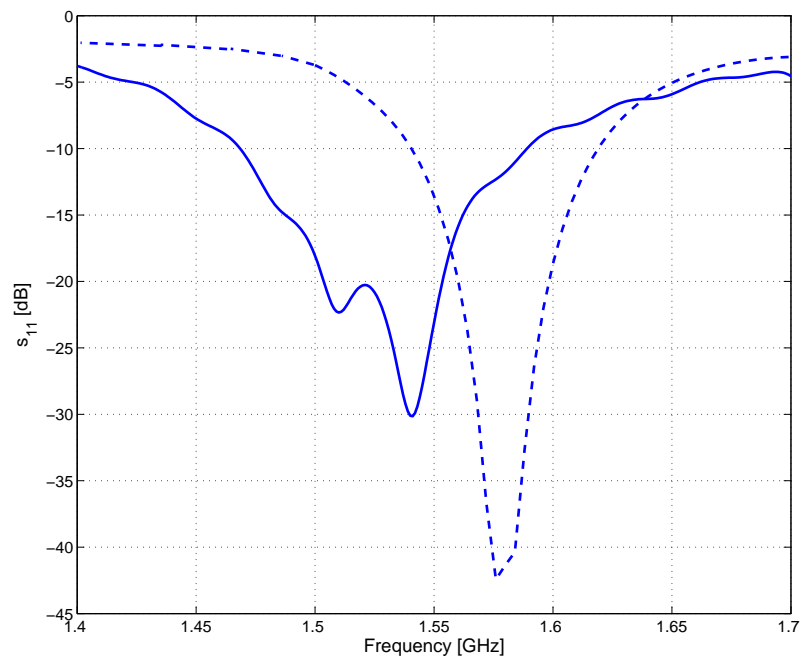


Figure 5.11: Measured and simulated s_{11} for the antenna.

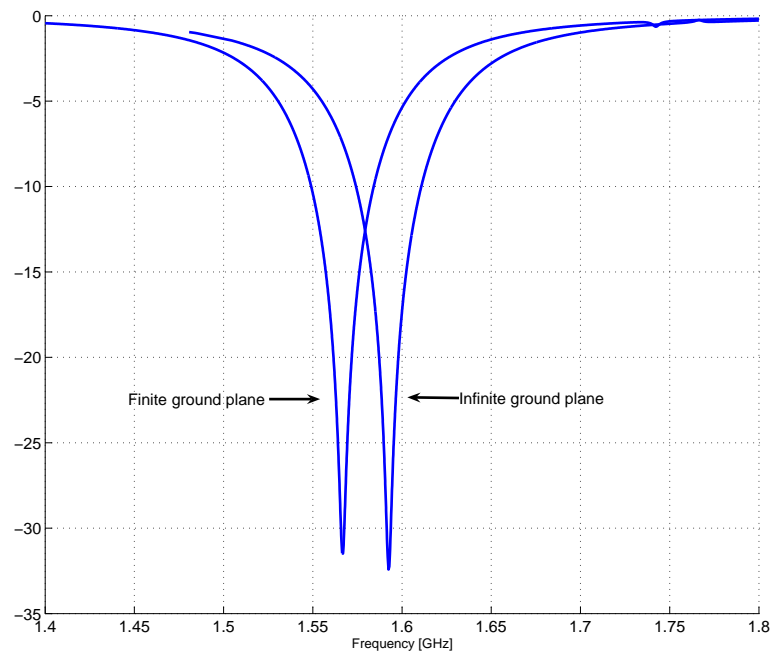


Figure 5.12: Simulated s_{11} for the antenna with an infinite and a finite ground plane.

5.6 Q of the single folded PIFA

It was shown in section 2.3.3 that the commonly used relation between fractional bandwidth and Q-factor, $BW = Q^{-1}$ does not hold true. To calculate the Q-factor of the single folded PIFA of figure 4.3 the equivalent circuit approach, as used by Chu (3) to define the fundamental limit on radiation Q, is used. The equivalent circuit of figure 5.13 is proposed to model the impedance response of the antenna.

The inductor, L_{feed} represents the mostly inductive pin feed, while the capacitor, C_{patch} models the capacitance between the patch and ground as well as the capacitance between the feed pin and the shorting plate. The inductor, L_{patch} represents the inductance of the patch. The capacitor, C_{rad} and the resistor, R_{rad} models the radiating edge of the PIFA.

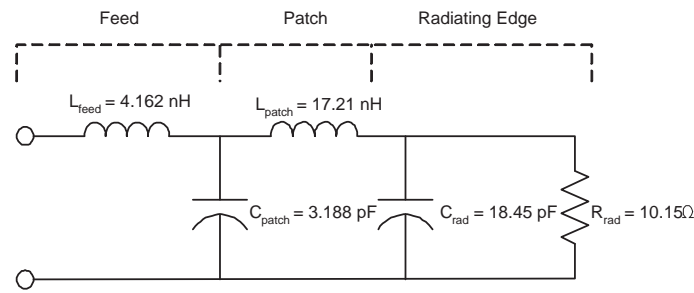


Figure 5.13: Equivalent circuit for the single folded PIFA.

Figure 5.14 shows the input impedance of the equivalent circuit and the simulated input impedance for the single folded PIFA. Near the resonant frequency of $1.61GHz$ the two input impedances are very similar.

This equivalent circuit was fed by a $1V$ source with a 50Ω source resistance and at a frequency of $1.61GHz$. From this the currents through all elements were calculated. The inductors store magnetic energy and the capacitors store electric energy. The average energy stored by an element is given by

$$W_m = \frac{1}{4} |I|^2 L$$

$$W_e = \frac{1}{4} |I|^2 \frac{1}{\omega^2 C}$$
(5.6.1)

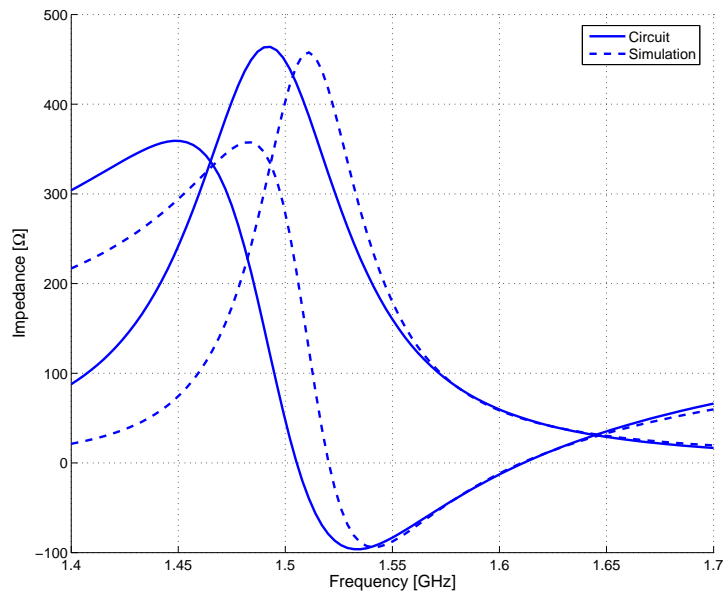


Figure 5.14: Simulated impedance and impedance of the equivalent circuit for the single folded PIFA.

where W_m is the average magnetic energy stored by an inductor and W_e is the average electric energy stored by a capacitor. The power radiated by the antenna is equal to the power dissipated in R_{rad} and is given by

$$P_{rad} = \frac{1}{2} |I|^2 R_{rad} . \quad (5.6.2)$$

At resonance the average stored magnetic and electric energies are equal and the Q-factor is given by

$$Q = \omega \frac{2W_m}{P_{rad}} . \quad (5.6.3)$$

This gave a Q-factor of 21.85 for the single folded PIFA, which has a relative size of $kr = 0.603$. Figure 5.15 shows this result along with the famous antenna by Goubau (12). The Q-factors of two electrically small dipoles of the same relative sizes are also given as reference along with the fundamental limits defined by Chu

(3) and McLean (7), as given by Hansen (1).

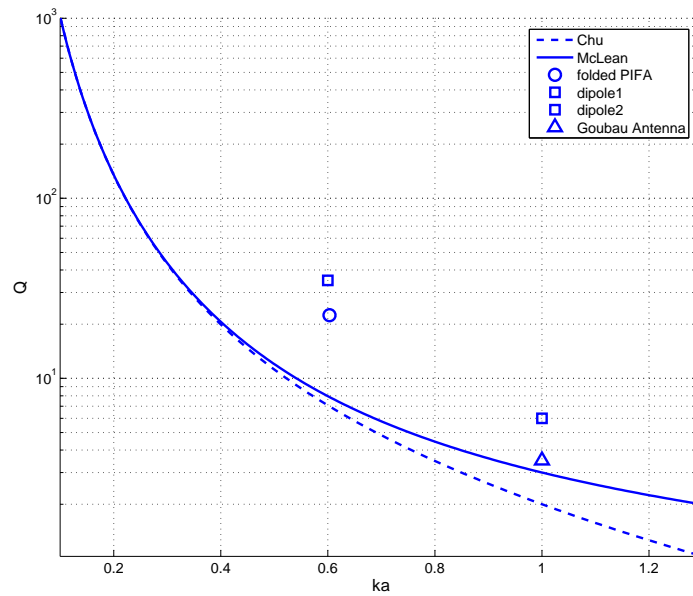


Figure 5.15: Q versus relative size for the folded PIFA and other electrically small antennas against the limits proposed by Chu and Mclean.

It is clear from the figure 5.15 that the Q -factor of the single folded PIFA is a significant improvement on the Q -factor of a dipole of equivalent relative size.

5.7 Arraying the antenna element

The antenna element is intended for use in a phase steered array and as such simulations of a 9-element rectangular array were conducted. To reduce the effect of mutual coupling between elements on the performance of the antenna, the elements were placed a half wavelength apart. Figure 5.16 shows the FEKO model of the 9-element rectangular array.

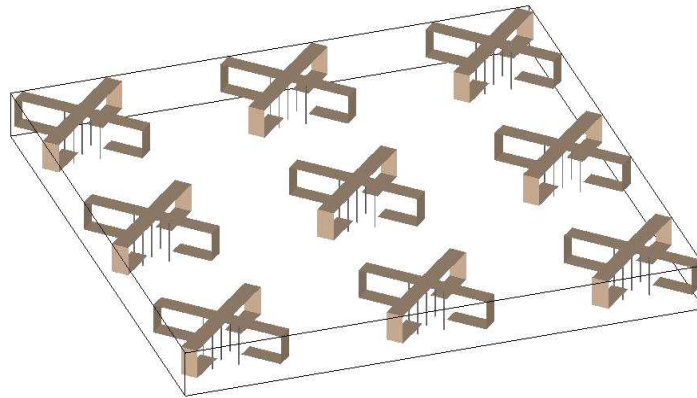


Figure 5.16: Simulation model of 9-element rectangular array.

By applying a different phase to each element the beam of the antenna is steered in the θ and ϕ directions. Figure 5.17 shows the simulated right-hand polarized gain of the 9-element rectangular array phase steered to $\theta = 45^\circ$. The gain of an single element is also shown.

With this array setup it was not possible to steer the main beam much wider than 60° . At these low angles the effect of the mutual coupling between the elements might be playing a role. This drop in performance can clearly be seen in figure 5.18,

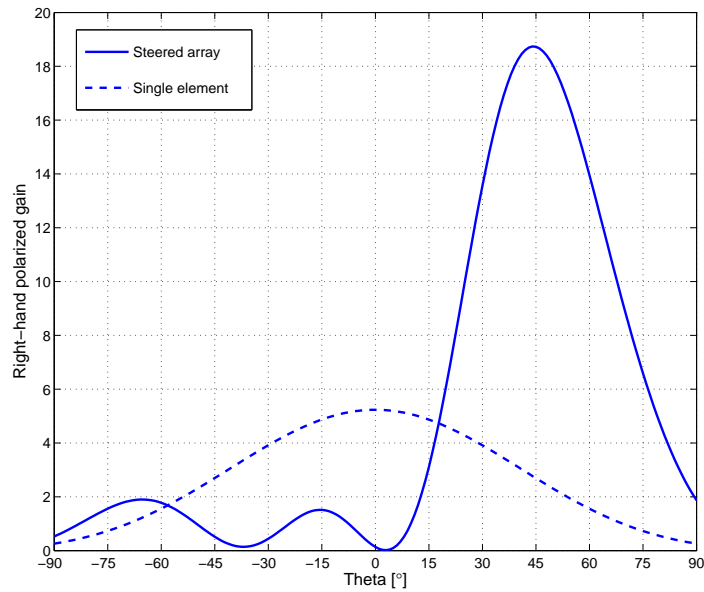


Figure 5.17: Right-hand polarized gain for the single element and the 9-element rectangular array phase steered to $\theta = 45^\circ$

where the array was phase steered to 85° . The main beam is directed at less than 60° and the reflected beam (at -60°) is also larger than in the case of the beam steered to 45° .

While the main beam can not be steered down to 85° , there is still a significant increase in the gain of the array compared to the single element at that low angle. As the simulation was conducted with an infinite ground plane the right-hand and left-hand simulated gain will be equal at 90° , limiting the array's performance at low scan angles. Just as the single measured element performs better than the simulation at low angles (see figure 5.9, p 59), the same could be expected from a constructed array with finite ground plane.

It is clear from the above that more work will have to be done on implementing the element in a wide-angle beam-steered array.

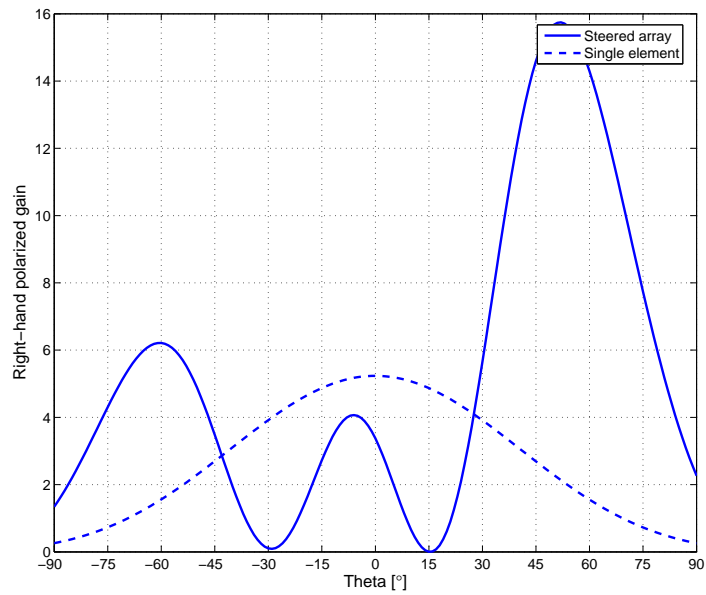


Figure 5.18: Right-hand polarized gain for the single element and the 9-element rectangular array phase steered to $\theta = 85^\circ$

Chapter 6

Conclusion

The effect of reducing the size of an antenna on its performance was illustrated by presenting the theoretical limits on the performance of electrically small antennas. Expressions for the theoretical limits on the bandwidth, gain and efficiency of electrically small antennas were presented. The radiation Q-factor of electrically small antennas was examined and, as it relates to bandwidth, this gave a fundamental limit on the bandwidth performance of an electrically small antenna. Similarly fundamental limitations were proposed for the achievable gain and efficiency of an electrically small antenna.

Through a study of the performance behavior of various electrically small antennas a more practical view of these performance limitations was presented. While many techniques have been used to reduce antenna size, it is clear that this size reduction can not be continued indefinitely.

From both the theoretical and practical examinations it became clear that much care should be taken when reducing the size of an antenna. Antenna engineers should always be mindful of the fundamental limitations of the antenna structures they are considering to avoid time wasted attempting to improve the performance of an electrically small antenna already performing close to its limits.

The design of an electrically small circularly polarized planar antenna element for use in a phase-steered array was presented successfully. By adapting the Pla-

nar Inverted-F Antenna an array of four sequentially rotated elements in a cross formation was fitted into the radian sphere to qualify the antenna as electrically small. The four arms of the antenna were fed with sequential phase shift to achieve circular polarization with the electrically small planar structure.

While the performance of this antenna is limited by the fundamental limitations on small antennas, an acceptable performance was achieved.

List of References

- [1] R. C. Hansen, "Fundamental limitations in antennas," *Proc. IEEE*, vol. 69, pp. 170-182. Feb. 1981.
- [2] H. A. Wheeler, "Fundamental limitations of small antennas," *Proc. IRE*, vol. 35, pp 1479-1484, Dec 1947.
- [3] L. J. Chu, "Physical limitations of omni-directional antennas," *J. Appl. Phys.*, vol. 19, pp. 1163-1175, Dec. 1948.
- [4] R. F. Harrington "Effect of antenna size on gain, bandwidth and efficiency," *J. Res. Nat. Bur. Stand.*, vol. 64-D, pp. 1-12, Jan./Feb. 1960.
- [5] R. E. Collin and S. Rothschild, "Evaluation of antenna Q," *IEEE Trans. Antennas Propagat.*, vol. 12, pp 23-27, Jan. 1964.
- [6] R. L. Fante, "Quality factor of general ideal antennas," *IEEE Trans. Antennas Propagat.*, vol. 17, pp 151-155, March 1969.
- [7] J. S. McLean, "A re-examination of the fundamental limits on the radiation Q of Electrically Small Antennas," *IEEE Trans. Antennas Propagat.*, vol. 44, pp. 672-676, May 1996.
- [8] D. M. Grimes and C. A. Grimes, "Minimum Q of electrically small antennas: a critical review," *Microwave Opt. Technol. Lett.*, vol. 28, pp 171-177, Feb. 2001.
- [9] G. A. Thiele *et al*, "On the lower bound of the radiation Q for electrically small antennas," *IEEE Trans. Antennas Propagat.*, vol. 51, pp 1263-1269, June 2003.
- [10] R. F. Harrington, *Time-Harmonic Electromagnetic Fields*. New York: McGraw-Hill, 1961.

- [11] G. S. Smith, "Efficiency of Electrically Small Antennas Combined with Matching Networks," *IEEE Trans. Antennas Propagat.*, vol. 25, pp 369-373, May 1977.
- [12] G. Goubau, "Multi-element monopole antennas," *Proc. Workshop on Electrically Small Antennas* ECOM, Ft. Monmouth, NJ, pp. 63-67, May 1976.
- [13] E. W. Seeley, "An experimental study of the disk-loaded folded monopole," *IRE Trans. Antennas Propagat.*, vol. 4, pp 27-28. Jan. 1956.
- [14] H. D. Foltz *et al*, "Disk-loaded monopoles with parallel strip elements," *IEEE Trans. Antennas Propagat.*, vol. 46, pp 1894-1896, Dec. 1998.
- [15] H. Choo and H. Ling, "Design of electrically small planar antennas using inductively coupled feed," *Electronics Letters*, vol. 39, Oct. 2003.
- [16] H. Choo *et al*, "Design of electrically small wire antennas using a Paterno genetic algorithm," *IEEE Trans. Antennas Propagat.*, vol. 53, pp 1038-1046, March 2005.
- [17] C. A. Balanis, *Antenna theory: analysis and design*, New Jersey: John Wiley & Sons, Inc., 1997.
- [18] R. B. Waterhouse, "Small microstrip patch antenna," *Electron. Lett.*, vol. 31, pp 604-605, Apr. 1995.
- [19] R. B. Waterhouse and S. D. Targonski, "Performance of microstrip patches incorporating a single shorting post," *Proc. IEEE Antennas Propagat. Symp.*, Baltimore, MD, pp 29-32, July 1996.
- [20] R. B. Waterhouse *et al*, "Improving the mechanical tolerances and radiation performance of shorted patches," *Proc. IEEE Antennas Propagat. Symp.*, Montreal, Canada, pp 1852-1855, July 1997.
- [21] R. B. Waterhouse *et al*, "Design and performance of small printed antennas," *IEEE Trans. Antennas Propagat.*, vol. 46, pp 1629-1633, Nov. 1998.
- [22] J. R. James, *Microstrip Antenna Theory and Design*. Stevenage, UK: Peter Peregrinus Ltd., 1981.
- [23] P. Salonen *et al*, "Single-feed dual-band planar inverted-F antenna with U-shaped slot," *IEEE Trans. Antennas Propagat.*, vol. 48, pp 1262-1264, Aug. 2000.

- [24] Y. Hwang *et al*, "Planar inverted F antenna loaded with high permittivity material," *Electron. Lett.*, vol. 31, pp 1710-1712, Sept. 1995.
- [25] Y. Li *et al*, "Broadband triangular patch antenna with a folded shorting wall," *IEEE Antennas Wireless Propagat. Lett.*, vol. 3, pp 189-192, 2004.
- [26] J. Row, "Dual-frequency triangular planar inverted-F antenna," *IEEE Trans. Antennas Propagat.*, vol. 53, pp 874-876, Feb. 2005.
- [27] C. R. Rowell and R. D. Murch, "A capacitively loaded PIFA for compact Mobile Telephone Handsets," *IEEE Trans. Antennas Propagat.*, vol. 45, pp 837-842, May 1997.
- [28] M. Sanad, "Effect of the shorting posts on short circuit microstrip antennas," *IEEE /AP-S International Symposium Digest*, pp. 701-704, Seattle, Washington, June 1994.